Linear Propagation and Absorption of the Fast Wave Near the First Ion Cyclotron Harmonic

M. Brambilla

IPP 5/52 August 1993

MAX-PLANCK-INSTITUT FÜR PLASMAPHYSIK

85748 GARCHING BEI MÜNCHEN

MAX-PLANCK-INSTITUT FÜR PLASMAPHYSIK

GARCHING BEI MÜNCHEN

Linear Propagation and Absorption of the Fast Wave Near the First Ion Cyclotron Harmonic

M. Brambilla

IPP 5/52 August 1993

Die nachstehende Arbeit wurde im Rahmen des Vertrages zwischen dem Max-Planck-Institut für Plasmaphysik und der Europäischen Atomgemeinschaft über die Zusammenarbeit auf dem Gebiete der Plasmaphysik durchgeführt.

LINEAR PROPAGATION AND ABSORPTION OF THE FAST WAVE NEAR THE FIRST ION CYCLOTRON HARMONIC.

M. Brambilla

Max–Planck–Institut für Plasmaphysik
Euratom Association
Garching bei München, Germany.

ABSTRACT

We investigate wave propagation and absorption in the vicinity of the first ion cyclotron harmonic resonance. Two regimes, dominated by mode conversion to Bernstein waves and by ion cyclotron damping, respectively, are identified, depending on the value of $k_{\|}$ and the density and temperature of resonant ions. With the help of analytic solutions of the fourth order finite Larmor radius (FLR) wave equations we derive simple expressions for the reflection and transmission of a fast wave impinging on the resonance, and for the efficiency of mode conversion through the resonance layer.

We also investigate the solutions of the second order wave equations obtained by order reduction. This approximation eliminates the short wavelength Bernstein waves, and replaces mode conversion by an equivalent power sink. As well–known, the reduced equations reproduce exactly the results of the full FLR wave equations if absorption at the "spurious" wave resonance is interpreted as mode conversion. We also show that the solutions of the order reduced equations can be used to obtain accurate estimates of direct ion cyclotron harmonic damping in the mode conversion regime. Absorption in the cyclotron damping regime can be obtained from the WKB solutions. Simple interpolation formulas covering both regimes are suggested, and compared with numerical results obtained with the FELICE code.

The results obtained can be used to evaluate the heating efficiency of a given antenna and for fast modeling of this heating scenario without extensive numerical calculations. Applications to ASDEX Upgrade and ITER are presented.

1 - Introduction.

Ion cyclotron heating at the first harmonic, $\omega = 2\Omega_i$, is an attractive heating scheme in the fusion reactor because of its insensitivity to the plasma composition: it can be applied to the optimal D–T plasma mixture without requiring further 'minority' species whose concentration could be difficult to control. Since its efficiency increases with the plasma pressure, it should perform at least as well as typical minority heating schemes if the ion temperature of the ohmic plasma exceeds 3 to 4 keV. At high power and low collisionality first harmonic heating is likely to produce tails of suprathermal ions, which might participate directly in fusion reactions and enhance the reactivity.

A disadvantage of first harmonic heating is that it requires a frequency twice as high as that for fundamental heating of the same species: this can imply more severe constraints for generators, transmission lines, and particularly for the antenna design. This disadvantage is minimized by heating the relatively heavy tritium: this choice also avoids parasitic absorption by α particles. On the other hand the higher frequency might offer more chances to non–conventional launcing structures, such as resonant cavities or folded waveguides, which might be better compatible with the reactor environnement.

In medium size tokamaks first harmonic heating is usually more difficult to implement than minority heating because of the low temperature of the ohmic plasma. This can be circumvented using some pre–heating, for example by neutral beam injection, which is usually also available on experimental tokamaks. Also, as well–known, first harmonic heating of deuterium should be avoided, because it is next to impossible to avoid contamination by some hydrogen, which tranforms the scenario into a typical minority heating one.

As most ion cyclotron heating scenarios, first harmonic heating in tokamaks is implemented by launching the fast (compressional) cold plasma wave (FW); the frequency is chosen to coincide with the first harmonic ion cyclotron frequency close to the plasma center. Two mechanisms compete to damp the fast wave in the vicinity of the resonance, namely ion cyclotron absorption and mode conversion to the lowest ion Bernstein wave. Elsewhere, Transit Time damping by the electrons can also be of importance if the electron temperature is large enough. Here, however, we will concentrate on wave propagation and absorption in the vicinity of the ion resonance.

Mode conversion near the first harmonic cyclotron resonance is a consequence of a confluence between the fast wave and the first ion Bernstein wave (IBW) [1]. The latter is a nearly electrostatic wave which propagates at frequencies just below $2\Omega_{ci}$, i.e., in the tokamak, on the high field side of the cyclotron resonance. The confluence occurs because near $\omega = 2\Omega_i$ the finite Larmor radius corrections to the dielectric tensor shows a 'resonant' behaviour. This decreases the wavevector of the hot plasma wave, while the wavevector of the FW, which depends only on the cold plasma contributions to the

dielectric tensor, is not affected by the resonance. The IBW is a backward wave, so that, if dissipation is weak, the confluence causes a narrow frequency gap in which both waves are evanescent. In the tokamak there is a region of evanescence just to the high field side of the cyclotron resonance, which screens waves launched from the low field side from the mode conversion layer. This effect was discovered by Weynants [2], who pointed out that the width of the evanescence region increases, hence the efficiency of mode conversion decreases, with increasing plasma pressure.

The IBW excited by mode conversion propagates toward higher magnetic fields, i.e. *away* from the cyclotron resonance, with rapidly decreasing wavelength. Ion cyclotron absorption of this wave therefore does not occur. Although a detailed investigation of the damping of the IBW is not easy, it is nevertheless clear that the associated power flux is finally thermalised. This will occur through Electron Landau damping if the parallel wavenumber increases sufficiently due to refraction in the non–uniform tokamak configuration [3]. Alternatively, if $k_{\|}$ remains too small, IBWs can be absorbed by stocastic ion heating as soon as their perpendicular wavelength becomes shorter than the thermal ion Larmor radius. This effect is not described by the linear theory of wave propagation, but is well documented by numerical studies [4], and can easily be taken into account in numerical solutions of the wave equations [5]. Mode conversion must therefore in any case be regarded as an energy sink for the externally launched FW; its effects on the power balance between species, on power deposition profiles, and on the distribution functions, however, are more difficult to investigate than those of direct ion harmonic damping, and are not yet fully understood.

A true confluence giving rise to mode conversion, however, occurs only when IC damping is weak, i.e. for nearly perpendicular propagation. For larger values of $n_{\|}$ the Doppler broadened region of strong cyclotron damping and the evanecence domain overlap, so that the two roots of the dispersion relation miss each other in the complex plane. This suppresses mode conversion in favour of direct cyclotron absorption. For a single mode, therefore, one can speak of two regimes, dominated by mode conversion or by cyclotron damping, respectively, depending on the value of $n_{\|}$ and on the density and temperature of the resonant ions.

These concepts, of course, should not be applied without qualification to heating experiments as a whole. The $n_{\|}$ spectrum of typical FW antennas is always broad enough to cover both regimes. In the case of antennas with more than one conductors, which allow some spectral shaping, mode conversion can be further suppressed by chosing an antisymmetric configuration. It is useful to have simple and reliable formulas for the efficiency of the various damping mechanisms as functions of $n_{\|}$: by folding them with the expected antenna power spectre, one can rapidly estimate of the performances of a given heating experiment, before performing extensive numerical simulations.

The plan of this report is as follows. In the next section we write down the finite Larmor radius (FLR) wave equations appropriate for the situation of interest, and we discuss the corresponding dispersion relation and the WKB solutions. In section 3 the FLR wave equations are solved by contour integrals in the limit of small ion cyclotron damping. The comparison of the asymptotic behaviour of these solutions with the WKB solutions provides connection formulas from which the fraction of power transmitted, reflected and mode converted are obtained. Similar connection formulas have been obtained by many Authors for transit through ion–ion resonances [6]–[7]. The wave equations near a first harmonic resonance, however, have a somewhat different structure, and slightly different techniques must therefore be used [8]–[9]. Nevertheless the results are of the well–known "Budden" type [10], and are expressed in terms of the optical thickness of the evanescence layer, just as those obtained for ion–ion resonances.

In section 4 we discuss the application of the order reduction technique [11] to the present problem. The reduced wave equations are of second order, since IBWs are eliminated, and can be solved in terms of Whittaker functions. As in other applications of order reduction, the connection formulas thus obtained give exactly the same power balance between transmission, reflection and absorption as the fourth order FLR wave equations, provided absorption is identified with mode conversion. The corresponding power sink in the reduced equations is due to a "spurious" wave resonance localized near the layer where mode–conversion would take place. This wave resonance is of a rather unphysical kind, since it corresponds to a singularity of both the electric and magnetic field of the waves which satisfy causality at infinity (true wave resonances usually give rise to logarithmic singularities only in the wave magnetic field). Nevertheless the domain in which the solutions of the reduced equations cannot be trusted is quite thin, and does not extend to the position of the ion cyclotron resonance. In section 5 we use this circumstance to estimate direct ion cyclotron absorption in the mode conversion regime. Ion cyclotron absorption in the limit of large $k_\parallel$ is obtained using the WKB solutions, and formulas interpolating between the two regimes are suggested. They compare very well with numerical results. These formulas provide a complete elementary description of linear fast wave propagation and absorption near a first harmonic ion cyclotron resonance.

In section 6, the analytic results are illustrated with applications to ASDEX Upgrade and ITER. The plasma parameters are summarized in Table 1. Those of the ASDEX Upgrade case are below the nominal performances of this device: they have been chosen as an example of the rather "unfavorable" low density, low temperature target plasmas available in medium size tokamaks. First harmonic heating can nevertheless be successful if the ohmic temperature can be raised to about 2 keV. The parameters of ITER have been adapted from the recommendations of the European Group on ICR Heating and Current Drive for code validations. Conclusions are summarized in section 7.

2. – Wave equations and dispersion relation.

2.1 – Finite Larmor Radius wave equations near the first harmonic cyclotron resonance. Cyclotron harmonic damping and mode conversion to the ion Bernstein wave can be quantitatively investigated by solving the wave equations in plane–stratified geometry in the FLR approximation. The correct form of these equations has been obtained by [12]–[16]. Neglecting for simplicity the electron inertia, and keeping only the h.f. FLR ion current which is "resonant" near $\omega = 2\Omega_i$, these equations can be written (lengths are measured in units of $k_o = \omega/c$)

$$\begin{aligned} 0 = &- \left(\frac{d}{dx} + n_y\right)\left[\lambda_2\left(\frac{d}{dx} - n_y\right)E_+\right] \\ &+ \left[n_z^2 - L - \frac{1}{2}\left(\frac{d^2}{dx^2} - n_y^2\right)\right]E_+ + \frac{1}{2}\left(\frac{d}{dx} - n_y\right)^2 E_- \qquad (1) \\ 0 = &+ \frac{1}{2}\left(\frac{d}{dx} + n_y\right)^2 E_+ + \left[n_z^2 - R - \frac{1}{2}\left(\frac{d^2}{dx^2} - n_y^2\right)\right]E_- \end{aligned}$$

where

$$R \simeq \sum_{ions} \frac{\omega_{pj}^2}{\omega^2}\frac{\Omega_{cj}}{\omega}\left(\frac{\omega}{\omega + \Omega_{cj}}\right) \qquad L \simeq -\sum_{ions} \frac{\omega_{pj}^2}{\omega^2}\frac{\Omega_{cj}}{\omega}\left(\frac{\omega}{\omega - \Omega_{cj}}\right) \qquad (2)$$

are non-resonant and of order zero in the Larmor radius (electron contributions have been taken into account through charge neutrality), while

$$\lambda_2 = \frac{1}{2}\sum_{\alpha} \frac{\omega_{p\alpha}^2}{\Omega_{c\alpha}^2}\frac{v_{th\alpha}^2}{c^2}\left\{ - x_{0\alpha} Z(x_{+2\alpha})\right\} \qquad (3)$$

is the finite Larmor correction resonant near $\omega = 2\Omega_i$; here

$$x_{+2\alpha} = \frac{\omega - 2\Omega_{c\alpha}}{k_\parallel v_{th\alpha}} \qquad (4)$$

and $Z(x)$ is the Plasma Dispersion Function. For large argument $-x\,Z(x) \to 1$, so that

$$\lambda_2 = \frac{1}{2}\sum_{\alpha} \frac{\omega_{p\alpha}^2}{\Omega_{c\alpha}^2}\frac{v_{th\alpha}^2}{c^2}\frac{\omega}{\omega - 2\Omega_{c\alpha}} \qquad \left|\frac{\omega - 2\Omega_{c\alpha}}{k_\parallel v_{th\alpha}}\right| \gg 1 \qquad (5)$$

We stress again that the resonant behaviour at $\omega = 2\Omega_{ci}$ shown by this coefficient singles out λ_2 among all other FLR contributions to the dielectric tensor, and justifies the approximations made to write Eq. (1). In a tokamak we will rerite (5) as

$$\lambda_2 = \frac{\hat{\lambda}_2}{x} \qquad \hat{\lambda}_2 = \frac{1}{2}\beta_{i_h}(k_o R_o) \qquad (6)$$

where R_o is the position of the harmonic cyclotron resonance, x the horizontal distance from R_o, and only the contribution of the heated species has been retained.

2.2 - The Dispersion Relation. The first step in the investigation of the wave equation is to discuss the local dispersion relation, which can be immediately obtained by assuming that the coefficients of Eqs. (1) are constant, and inserting a plane–wave solution. With $d/dx \to in_x$, $n_x^2 + n_y^2 = n_\perp^2$, we obtain

$$\frac{\lambda_2}{2} n_\perp^4 + \left[(n_z^2 - S) + (n_z^2 - R)\lambda_2\right] n_\perp^2 + (n_z^2 - R)(n_z^2 - L) = 0 \tag{7}$$

Exactly this equation can be obtained from the full hot–plasma dispersion relation by expanding in the Larmor radius, neglecting the electron inertia, and keeping only the ion FLR term which is resonant at $\omega = \Omega_{ci}$. The importance of some of the omitted terms will be estimated below by comparing the solutions of this "reduced" dispersion relation with those of the complete FLR and of the full hot–plasma dispersion relations.

We will abbreviate

$$\nu_A^2 = n_\parallel^2 - A \qquad\qquad q_F^2 = -\frac{\nu_R^2 \nu_L^2}{\nu_S^2} \tag{8}$$

so that q_F is the asymptotic perpendicular index of the FW. We assume that B_o increases to the left; then $\nu_L^2 > 0$, $\nu_R^2 < 0$, but $\nu_S^2 = (\nu_R^2 + \nu_L^2)/2 > 0$, so that the fast wave is propagative, $q_F^2 > 0$; we will actually assume $q_F^2 > n_y^2$ to have real wave fronts. With these notations, the two solutions of Eq. (7), developed for $|\lambda_2| \ll \nu_S^2$, are

$$n_\perp^2 = \simeq -\frac{\nu_R^2 \nu_L^2}{\nu_S^2} \frac{1}{1 + q_F^2 h_F^2 \, (\lambda_2 / 2\nu_S^2)} \simeq q_F^2 \left[1 - \frac{1}{2}\left(\frac{\nu_R^2}{\nu_S^2}\right)^2 \frac{\hat{\lambda}_2}{x}\right] \tag{9}$$

for the FW, and

$$n_\perp^2 \simeq -\left(\frac{2\nu_S^2}{\lambda_2} + 2\nu_R^2\right) + \frac{\nu_R^2 \nu_L^2}{\nu_S^2} = -\frac{2\nu_S^2}{\hat{\lambda}_2} x - q_F^2 \, h_F^2 \tag{10}$$

for the BW. Here

$$h_F^2 = -(\nu_R^2 / \nu_L^2) > 0 \tag{11}$$

The shear cold–plasma wave has been eliminated by the zero electron inertia approximation; it can be shown that this is justified as long as the very mild condition

$$\beta = \frac{8\pi n T}{B_o^2} \gtrsim \frac{m_e}{m_i} \tag{12}$$

is satisfied.

The factorization (9)–(10) breaks down near the first ion cyclotron harmonic. The confluence between the two roots which occurrs there is due to the resonant behaviour of the FLR term λ_2; this is in contrast to usual wave resonances, which are due to zeros of the cold–plasma coefficient ν_S^2. In spite of this difference, mode conversion and wave propagation near $\omega = 2\Omega_i$ are essentially the same as near ordinary wave resonances.

The roots of the dispersion relation (7) near $\omega = 2\Omega_{ci}$ in a typical ASDEX Upgrade plasma are shown in fig. 1 for perpendicular propagation, and in figs 2 and 3 for oblique propagation. Note that in the limit of perpendicular propagation there is an effective cut–off for the Bernstein branch at the cyclotron resonance. The dispersion curves for ITER are similar: the evanescence region is broader, as expected, although much less than in proportion to the major radius R_o: 15 cm if Deuterium is heated, and only 4 cm if Tritium is heated at 10 keV in a 50%–50% mixture (this is due to the dependence of $\hat{\lambda}_2$, L and R on the charge to mass ratio of the resonant ions). The broadening of the evanescent region at perpendicular propagation with increasing β is illustrated in fig. 4 for the case of f.h. heating of Tritium in ITER.

2.3 – Mode conversion versus cyclotron damping. Figures 1 to 3 also illustrate the transition from the mode–conversion regime to the cyclotron harmonic regime mentioned in the introduction, due to the progressive widening of the cyclotron damping region at the expense of the evanescence region as $n_\parallel$ increases. We can derive the conditions for this transition as follows. Let us first consider nearly perpendicular propagation (i.e. $n_\parallel$ so small that coefficients in Eq. (1) are real). Then we can locate the region of evanescence and the confluences between the two waves by asking for the values of λ_2 which make the discriminant of the DR vanish. Using for λ_2 its expression in the limit of perpendicular propagation, Eq. (6), this gives

$$\frac{\omega - 2\Omega_{ci}}{\omega} = -\beta_i \frac{h_F^2}{1 \pm \sqrt{h_F^2}} \tag{13}$$

Since $h_F^2 < 1$, the evanescence region lies to the high field side of the resonance, as anticipated. The horizontal thickness of the evanescence layer is proportional to the toroidal radius R_o and the ion $\beta_i = (\omega_{pi}^2/\Omega_{ci}^2)\cdot(v_{thi}^2/c^2)$. Both factors are of course much larger in a reactor–like plasma than in a medium size tokamak. Since the wavelength of the fast wave is rather insensitive to the plasma parameters, we can anticipate the optical thickness of the layer to be also be greater in the reactor case. As seen above, however, the dependence of h_F^2 on the plasma composition can partially compensate for this effect.

The layer where ion cyclotron harmonic is not negligible, on the other hand, is characterized by the inequality

$$\left|\frac{\omega - 2\Omega_{ci}}{\omega}\right| \lesssim q|n_\parallel|\frac{v_{thi}}{c} \tag{14}$$

where q is a number of order unity (between 2 and 3). Mode conversion will occur, roughly speaking, if this layer does not extend beyond the midpoint between the two confluences. This gives the condition

$$\beta_i \frac{h_F^2}{1-h_F^2} \gtrsim q|n_\parallel| \frac{v_{thi}}{c} \tag{15}$$

The l.h. side grows faster than the r.h. side with the plasma temperature, and is moreover proportional to the plasma density, which does not enter in the r.h. side. Since the values of $n_\parallel$ which can be launced by IC antennas are nearly independent on the plasma size, this condition will be more easily satisfied with increasing plasma performances. It has been pointed out [2] that this circumstance might somewhat reduce the efficiency of cyclotron harmonic damping in the reactor. It turns out, however, that for waves excited from the low field side, which encounter first the cyclotron harmonic, this is only a minor effect.

We can define a critical parallel wavenumber for the transition from the mode conversion regime to the cyclotron harmonic regime as the value of $n_\parallel$ for which condition (15) is satisfied with, say, $q = 2$. We have plotted the required $n_\parallel$ in fig. 5 for ASDEX Upgrade, and in figs. 6 for ITER at the first harmonic of tritium. As expected, the critical value of $n_\parallel$ increases with temperature; in all cases however it remains relatively small throughout the range of admissible ion temperatures. Clearly, for any reasonable antenna, only a fraction of the launced spectrum will be in the mode conversion regime, even in the case of a monopole configuration (spectrum centered on $n_\parallel = 0$); with a dipole (antisymmetric) antenna this fraction can easily be made negligible.

It is also interesting to compare the simplified FLR dispersion relation (7) with the full hot–plasma dispersion relation. Indirectly, this gives also an idea of the accuracy of the wave equation (1). Eq. (7) turns out to be very accurate (better than 1%) for perpendicular propagation, and only slightly less for values of $n_\parallel$ above the transition to the cyclotron damping regime. In this regime, the imaginary part of the FW index is slightly overestimated (by a few %), and the imaginary part of the BW index underestimated (by 10 to 20%). The origin of these inaccuracies is the omission of electron FLR terms (in particular in $\epsilon_{yz} = -\epsilon_{zy}$), rather than a breakdown of the FLR approximation. The numerical solution of the full FLR wave equations, which takes these terms into account, should therefore give very good results in all cases.

2.4 – WKB solutions. In the following we will need rather detailed WKB solutions to the wave equations (1). We write these WKB solution in the following form:

$$E_j(x) = \sum_\alpha \frac{1}{p_\alpha^{1/2} W_\alpha} \left[A_a G^+_{\alpha j} e^{i\int^x p_\alpha \, dx} + B_a G^-_{\alpha j} e^{-i\int^x p_\alpha \, dx} \right] \tag{16}$$

Here $j \in \{+,\ -\}$ is used to denote components, and $\alpha \in \{F,\ B\}$ to label the two roots p_α^2 of the dispersion relation for n_x, i.e.

$$p_\alpha^2 = q_\alpha^2 - n_y^2 \tag{17}$$

Moreover A_α, B_α are arbitrary constants; $W_\alpha(x)$ are the WKB amplitude factors; and $G^\pm_{\alpha j}(x)$ are the polarisation factors. We will chose p_α so that the first term always carries energy or decreases exponentially towards the left (hence $p_\alpha = -\sqrt{p_\alpha^2}$ for backward waves, $p_\alpha = i\sqrt{-p_\alpha^2}$ for evanescent waves). The polarization factors $G^\pm_{\alpha j}(x)$ must satisfy

$$G^\pm_{\alpha,+} = \frac{(p_a \pm i n_y)^2}{q_\alpha^2 + 2(\nu_L^2 + \lambda_2)} G^\pm_{\alpha,-} = \frac{q_\alpha^2 + 2\nu_R^2}{(p_a \mp i n_y)^2} G^\pm_{\alpha,-} \tag{18}$$

The WKB factors W_α, finally, will be chosen so that in the propagative case the wave carries a unit of energy per unit area. For this purpose, we need the general expression for the power flux within the WKB approximation, namely

$$P_x + T_x = \frac{\omega}{8\pi}\left\{ \mathrm{Re}\,(p_\alpha)\,|E_y|^2 - n_y\,\mathrm{Re}\,(E_y^* E_x) - \mathrm{Re}\,(p_a\,\lambda^{2,i})\,|E_+|^2 \right\} \tag{19}$$

The last term, T_x, is the kinetic power flux arising because of spatial dispersion.

A) Fast wave. For the FW, to lowest order ($\lambda_2 \to 0$), we write

$$G^\pm_{F,+} \simeq \zeta_\pm\, G^\pm_F = -\frac{\nu_R^2}{\nu_L^2}\zeta_\pm \qquad\qquad G^\pm_{F,-} = \zeta_\mp \tag{20}$$

where the factors

$$\zeta_\pm = \frac{q_F}{p_F \mp i n_y} = \frac{p_F \pm i n_y}{q_F} \qquad\qquad |\zeta_\pm|^2 = \zeta_+\,\zeta_- = 1 \tag{21}$$

are close to unity for $n_y^2 \ll q_F^2$. Inserting in Eq. (19) and taking into account that the kinetic flux is negligible for the fast wave, we have

$$W_F^2 = \frac{1}{2}|\zeta_\mp - \zeta_\pm\, G_F^\pm|^2 \mp \frac{n_y}{p_F}\,\mathrm{Im}\,(G_F^\pm) = \frac{1}{2}\left(1 - h_F^2\right)^2 = 2\left(\frac{\nu_S^2}{\nu_L^2}\right)^2 \tag{22}$$

B) Bernstein wave. For the BW, in the same approximation, we can write

$$G^\pm_{B,+} \simeq 1 \mp i\frac{n_y}{p_B} \qquad\qquad G^\pm_{B,-} \simeq 1 \pm i\frac{n_y}{p_B} \tag{23}$$

where we have taken into account that $n_y^2 \ll q_B^2$. This coincides with the electrostatic approximation. As a consequence, the flux associated with the Bernstein wave is dominated by the kinetic part. Substituting into (19) we get

$$W_B^2 = \left\{ |G_B^\pm|^2 \mp \frac{n_y}{p_B}\,\mathrm{Re}\,(G_B^\pm) - \frac{\lambda_2}{2}|1 + iG_B^\pm|^2 \right\} \simeq -\frac{\lambda_2}{2} \tag{24}$$

The four independent solutions thus normalized, obtained by taking one of the four constants A_α, B_α in turn equal to unity and the others zero, will be called the *reference* WKB solutions. Using Eqs. (9), (10), and (6) (which always hold in the WKB region), and taking into account that the BW is a backward wave, these solutions can be written

$$\vec{E}_F^{\pm} = \frac{1}{(2p_F)^{1/2}\nu_S^2}\left\{\zeta_\pm \nu_R^2\,\vec{u}_+ - \zeta_\mp \nu_L^2\,\vec{u}_-\right\} \exp\left\{\pm i\left[p_F x - \frac{q_F^4 h_F^2}{2p_F}\left(\frac{\hat{\lambda}_2}{2\nu_S^2}\right)\ln\left(2p_F|x|\right)\right]\right\} \tag{25}$$

$$\vec{E}_B^{\pm} = \frac{1}{(2\nu_S^2)^{1/2}}\left(\frac{2\nu_S^2}{-\hat{\lambda}_2}\right)^{1/4}(-x)^{1/4}\left\{\zeta_\mp\,\vec{u}_+ + \zeta_\pm\,\vec{u}_-\right\} \exp\left\{\mp i\frac{2}{3}\left(\frac{2\nu_S^2}{\hat{\lambda}_2}\right)^{1/2}(-x)^{3/2}\right\}$$

Here the superscripts $+$, $-$ denote the wave propagating towards the left, to the right, respectively. The amplitude of the BW solution increases toward the left to compensate for the decrease in group velocity.

3 – Solution of the wave equations for nearly perpendicular propagation.

3.1 – Solution by Laplace integrals. Analytic solutions to the wave equations (1) can be obtained only for nearly perpendicular propagation, so that cyclotron damping can be neglected, and λ_2 is given by Eq. (6). Compared with the rapid variation of the resonant term λ_2, we can neglect the space dependence of R and L. Then, eliminating E_-, we obtain the single fourth–order wave equation

$$0 = \left[-\frac{1}{2}\left(\frac{d^2}{dx^2} - n_y^2\right) + \left(n_z^2 - R\right)\right]\left\{\left(\frac{d}{dx} + n_y\right)\left[\frac{\hat{\lambda}_2}{x}\left(\frac{d}{dx} - n_y\right)E_+\right]\right\} + \left(\frac{d^2}{dx^2} - n_y^2\right)\left[\left(n_z^2 - S\right)E_+\right] - \left(n_z^2 - R\right)\left(n_z^2 - L\right)E_+ \tag{26}$$

Solutions of this equations can bew written in the form of Laplace integrals,

$$E_+^i(x) = \int_{C_i} \Lambda(p) e^{\Psi(x,p)}\,dp \tag{27}$$

along appropiate contours C_i. With some simple algebra one finds

$$\Lambda(p) = \left(1 - \frac{q_F^2 h_F^2}{p^2 + p_F^2}\right)(p + n_y)$$

$$\Psi(x,p) = \left(x + \frac{\hat{\lambda}_2}{2\nu_S^2}\alpha\right)p - \frac{\hat{\lambda}_2}{2\nu_S^2}\frac{p^3}{3} + i\frac{\eta}{\pi}\ln\frac{(p - ip_F)}{(p + ip_F)} \tag{28}$$

where

$$p_F = \sqrt{q_F^2 - n_y^2} = q_F\,\zeta_y \qquad \zeta_y = \sqrt{1 - (n_y^2/q_F^2)} \tag{29}$$

is the asymptotic horizontal index of the Fast Wave,

$$\eta = \pi\,\frac{\hat{\lambda}_2}{2\nu_S^2}\,\frac{q_F^4\,h_F^2}{2p_F} = \frac{\pi}{8}\beta_i(k_o R_o)\left(\frac{\nu_R^2}{\nu_S^2}\right)^2\frac{q_F}{\zeta_y} \tag{30}$$

is the *optical thickness* of the evanescence layer between the effective cut–off at the cyclotron harmonic resonance and the mode conversion layer (cfr. above), and

$$\alpha = q_F^2\,h_F^2 + n_y^2 = 2(q_F^2 + \nu_R^2) - p_F^2 \tag{31}$$

The function $\tilde{E}_+(p)$ has an essential singularity at infinity, and branch singularities at $p = \pm i p_F$ on the imaginary axis. The main sheath can be defined by cutting the p–plane along the imaginary axis between these two points; the principal value of the logarithm is to be taken on the positive p–axis. Since $\hat{\lambda}_2/2\nu_S^2 > 0$, $\tilde{E}_+(p) \to 0$ for $|p| \to \infty$ in the directions such that

$$\cos 3\phi_p > 0 \qquad\qquad \phi_p = \arg p \tag{32}$$

The contours C_i can go to infinity only within the sectors which satisfy this condition.

3.2 – Asymptotic behaviour of the solutions. The points of stationary phase of the integrand in Eq. (27) satisfy

$$\begin{aligned} p_{sp}^2 + p_F^2 &= \lambda_\pm^2(x) \\ &= \frac{\nu_S^2}{\hat{\lambda}_2}x + (q_F^2 + \nu_R^2) \pm \sqrt{\left[\frac{\nu_S^2}{\hat{\lambda}_2}x + (q_F^2 + \nu_R^2)\right]^2 + q_F^4\,h_F^2} \end{aligned} \tag{33}$$

(this notation does not imply $\lambda_\pm^2 \geq 0$ throughout; these functions are real for all x, however, and both are positive for large and negative x). We write the four saddle points described this equation as

$$p_\pm^u = +i\sqrt{p_F^2 - \lambda_\pm^2(x)} \qquad p_\pm^l = -i\sqrt{p_F^2 - \lambda_\pm^2(x)} \tag{34}$$

where the subscripts refer to their position in *upper* and *lower* halfplane when x is large and negative: in this case $p_+^{u,r}$ are on the imaginary axis just above (below) the branch points $\pm i p_F$, while $p_-^{u,r}$ are much farther away on the imaginary axis. When x is large and positive, $p_-^{u,r}$ move toward the branch points, remaining on the imaginary axis, while $p_+^{u,r}$ migrate to the real axis and approach $\pm\infty$. The two pairs of saddle points exchange their role when x goes through the resonance $x = 0$.

Four contours leading to four linearly independent solutions with well–defined asymptotic behaviour for $x < 0$ and for $x > 0$ are shown in fig. 7. Remembering that the Bernstein wave is a backward wave, the identifications are

A) $x < 0$		
C_B^u	Bernstein Wave propagating	towards $-\infty$
C_F^u	Fast Wave propagating	from $-\infty$
C_F^l	Fast Wave propagating	towards $-\infty$
C_B^l	Bernstein Wave propagating	from $+\infty$

B) $x > 0$		
D_B^u	Bernstein Wave evanescent	towards $+\infty$
D_F^u	Fast Wave propagating	to $+\infty$
D_F^l	Fast Wave propagating	from $+\infty$
D_B^l	Bernstein Wave growing	towards $+\infty$

To evaluate the asymptotic behaviours explicitly, however, we can use the saddle–point method only for the solutions representing Bernstein waves; for those representing fast waves the point of stationary phase is too close to the branch singularity, and the integrals are of the Hankel type instead.

A) Fast Wave–type solutions for large negative x. Let us first consider the integral along C_F^l. The integrand is dominated by the factor $e^{(p+ip_F)x}$ as long as

$$|p + ip_F| << \left(\frac{2\nu_S^2}{\hat{\lambda}_2}\right)^{1/2} (-x)^{1/2} \tag{35}$$

Hence for sufficiently large $-x > 0$, substituting $p = -ip_F - t/x$ in the exponential and putting $p = 0$ in all other factors, we can write

$$E_F^l(x) \simeq G_o \left(-\frac{1}{x}\right)^{-i\frac{\eta}{\pi}} \int_{C_H} e^{-t}\,(-t)^{-(1+i\frac{\eta}{\pi})}\,dt \tag{36}$$

where

$$G_o = -\frac{q_F^2\,h_F^2}{2}\left(1 + i\frac{n_y}{p_F}\right) e^{-\frac{\eta}{2}} \exp\left\{-i\left[\frac{\hat{\lambda}_2}{2\nu_S^2}\left(\alpha p_F - \frac{p_F^3}{3}\right) - \frac{\eta}{\pi}\ln(2p_F)\right]\right\} \tag{37}$$

and the countour C_H runs from $+\infty$ to the origin just above the real axis, encircles the branch point $s = 0$ counterclock–wise, and goes back to $+\infty$ just below the real axis. The integral can therefore be evaluated by comparison with Hankel identity for the Gamma function [12]. The integral along C_F^u is just the complex–conjugate. In this way, apart for a factor of modulus unity, these two solutions in the left asymtotic region are found to behave as the normalized WKB solutions $\vec{E}_F^{\pm}$ multiplied by the factor

$$\sqrt{2\pi}\, q_F^{1/2}\, \nu_R^2\, \frac{e^{-(\eta/2)}}{\Gamma\left(1 \pm i\eta/\pi\right)} \tag{38}$$

B) Fast Wave–type solutions for large positive x. The integrals along $D_F^{u,l}$ can be treated in the same way as the one along $C_F^{u,l}$. For sufficiently large $x > 0$ these two solutions in the left asymtotic region are found to behave as the normalized WKB solutions $\vec{E}_F^{\pm}$ multiplied by the factor

$$\sqrt{2\pi}\, q_F^{1/2}\, \nu_R^2\, \frac{e^{+(\eta/2)}}{\Gamma\left(1 \pm i\eta/\pi\right)} \tag{39}$$

again disregarding a factor of modulus unity.

C) Bernstein–type solutions for large negative x. We turn now to the integrals along $C_B^{u,l}$. For large negative x the corresponding saddle points p_-^u and p_-^l can be approximated as

$$p_-^{u,l} \simeq \pm i \left(-\frac{2\nu_S^2}{\hat{\lambda}_2} x \right)^{1/2} + O\left(|x|^{-1/2} \right) = \pm i q_B \tag{40}$$

The corresponding integrals can be approximated by

$$E_{B+}^{u,l}(x) \simeq \left(\frac{2\pi}{\Psi''_{u,l}} \right)^{1/2} \Lambda(p_-^{u,l})\, e^{\Psi(x, p_-^{u,l})} \tag{41}$$

provided that

$$\left| \frac{\Psi''}{2} (p_F - p_B)^2 \right| \simeq \left(\frac{2\nu_S^2}{\hat{\lambda}_2} \right)^{1/2} (-x)^{3/2} \gg 1 \tag{42}$$

a condition which is well satisfied in the WKB domain. Evaluating $\Lambda(p_-^{u,l})$, $\Psi(x, p_-^{u,l})$, and Ψ'', and taking into account that the logarithmic function takes its principal value at the right end of the paths $C_B^{u,l}$, we find that these two solution behave as the normalized WKB solutions $\vec{E}_F^{\pm}$ multiplied by the factor

$$(2\pi\nu_S^2)^{1/2} \left(\frac{2\nu_S^2}{\lambda_2} \right)^{1/2} e^{\pm i(3\pi/4)} \tag{43}$$

D) Bernstein–type solutions for large positive x. For large positive x the saddle points corresponding to Bernstein waves are $p_+^{u,l}$ are:

$$p_+^{u,l} = \pm \left(\frac{2\nu_S^2}{\hat{\lambda}_2} x \right)^{1/2} + O\left(x^{-1}\right) \tag{44}$$

The solutions evaluated along $D_B^{u,l}$ therefore behave asymptotically as

$$E_B^{u,l}(x) \simeq -\sqrt{\pi} \left\{ \begin{matrix} i \\ 1 \end{matrix} \right\} \left(\frac{2\nu_S^2}{\hat{\lambda}_2} \right)^{3/4} (x)^{1/4} \exp\left\{ \pm \frac{2}{3} \left(\frac{2\nu_S^2}{\hat{\lambda}_2} \right)^{1/2} x^{3/2} \right\} \tag{45}$$

Strictly speaking, the exponentially growing solution always picks up also a contribution from the other Bernstein–type saddle point, which however is subdominant, and can be neglected.

3.3 – Connection formulas. Connections formulas can now be obtained by noting that each of the solutions written above is regular for all finite x. The appropriate path can then be determined by imposing causality on the transmitted waves, and then deformed to determine the corresponding combination of incident and reflected waves.

A) Fast Wave incident from the low field side. Causality requires: 1) no wave carrying energy from $-\infty$; 2) no growing solution for $x > 0$. The first condition excludes the paths C_F^+ and C_B^+; the second can be satisfied by an appropriate combination of paths C_F^- and C_B^- which run through the forbidden saddle point, such that the contributions cancel each other. With the help of fig. 8a, it is not difficult to see that this requires that the integral along C_F^- be multiplied by the factor $1 - e^{-2\pi\eta}$, and the integral along C_B^- by $-(1 - e^{-2\pi\eta})$. The two paths can then be deformed as shown in fig. 8b to d. From fig. 8d, we recognize for large $x > 0$ the contributions from the incident fast wave E_F^- with weight 1, from the reflected fast wave with weight $1 - e^{-2\pi\eta}$, and from the evanescent BW also with weight $1 - e^{-2\pi\eta}$. Taking into account the asymptotic amplitudes of the different waves, but neglecting factors of modulus unity, we summarize these results as follows:

$$\begin{aligned} &\sqrt{2}\pi\, p_F^{1/2}\, \nu_R^2 \frac{e^{-(\eta/2)}}{\Gamma(1+i\eta/\pi)}\, E)_F^- \\ &\qquad - \left(1 - e^{-2\eta}\right) (2\pi\nu_S^2)^{1/2} \left(\frac{2\nu_S^2}{\lambda_2} \right)^{1/2} E)_B^- \qquad (x < 0) \\ \longleftrightarrow \quad &\sqrt{2}\pi\, p_F^{1/2}\, \nu_R^2 \left\{ \frac{e^{+(\eta/2)}}{\Gamma(1+i\eta/\pi)}\, E)_F^- \right. \\ &\qquad \left. + \left(1 - e^{-2\eta}\right) \frac{e^{+(\eta/2)}}{\Gamma(1-i\eta/\pi)}\, E)_F^+ \right\} \qquad (x > 0) \end{aligned} \tag{46}$$

(the evanescent BW for $x > 0$ has been omitted for simplicity, since it does not participate to power transport). We recall that the basic solutions $E)_\alpha^\pm$ are normalised to the same power flux, and that the incident wave is $E)_F^-$ for $x > 0$. Using a well–known identity for the modulus of the Γ function and the definition of η we finally obtain the coefficients of transmission, reflection and mode conversion:

$$\begin{aligned} \mathcal{R} &= (1 - e^{-2\eta})^2 \\ \mathcal{T} &= e^{-2\eta} \\ \mathcal{A} &= (1 - e^{-2\eta}) e^{-2\eta} \end{aligned} \tag{47}$$

B) Fast Wave incident from the high field side. We now must require: 1) no wave carrying energy from $+\infty$; 2) no growing solution for $x > 0$. A similar, but simpler, exercise leads to the following coefficients of transmission, reflection and mode conversion:

$$\begin{aligned} \mathcal{R} &= 0 \\ \mathcal{T} &= e^{-2\eta} \\ \mathcal{A} &= 1 - e^{-2\eta} \end{aligned} \tag{48}$$

The total energy is strictly conserved in both cases. As usual, mode conversion is more efficient for waves incident on the mode conversion layer from the high field side of the tokamak, which suffer no previous reflection at the effective cutoff.

4 – Order reduction for first harmonic heating.

The results (47) and (48) are formally identic with those obtained from the well–known Budden model [10], which is based on a second order wave equation displaying a resonance and a cutoff. This suggests to simplify the fourth order wave equations (26) by suppressing the short wavelength BWs, replacing mode conversion by an equivalent power sink. This procedure is known as "order reduction algorithm" [11]. The resulting second order wave equations is easily solved in terms of classic analytic functions; this will be useful in the next subsection to estimate cyclotron damping. Order reduction in this context is also of interest because the solutions of the fourth order wave equations are known in closed form, at least for quasi–perpendicular propagation. Thus a direct comparison of the 'exact' and 'reduced' equations is possible.

We perform order reduction by substituting the wavevector $k_x = p_F$ for $-i(d/dx)$ in the outer second order operator of the first term in Eq. (26). This tranform the wave equations into a single second order equation

$$\epsilon^2 \left(\frac{d}{dx} + n_y \right) \left[\frac{1}{x} \left(\frac{d}{dx} - n_y \right) E_+ \right] + \left(\frac{d^2}{dx^2} + p_F^2 \right) E_+ = 0 \tag{49}$$

with

$$\epsilon^2 = q_F^2 h_F^2 \frac{\hat{\lambda}_2}{2\nu_S^2} = \frac{1}{4}\beta_i(k_o R_o)\left(-\frac{\nu_R^2}{\nu_S^2}\right)^2 = \frac{2p_F}{q_F}\frac{\eta}{\pi} \tag{50}$$

The dispersion relation (as usual with $n_\perp^2 = n_x^2 + n_y^2$) is now

$$n_\perp^2 = \frac{q_F^2}{1 + (\nu_R^2/\nu_S^2)^2(\lambda_2/2)} \tag{51}$$

Comparison with Eq. (9) shows that Eq. (49) describes the FW including FLR corrections, but not the Bernstein wave, as expected. The confluence with the latter is replaced by a singularity at the point $x = -\epsilon^2$ (the cyclotron harmonic resonance at $x = 0$ gives rise to a peculiar behaviour of the polarization, but the equation itself is regular there).

Of course, Eq. (49) could be solved with Laplace integrals. It is however more useful to have solutions in terms of known analytic functions. For this purpose, let

$$E_+ = \left(\frac{d}{dx} + n_y\right) F \tag{52}$$

Then Eq. (49) becomes

$$\left(\frac{d}{dx} + n_y\right)\left\{\left(1 + \frac{\epsilon^2}{x}\right)\frac{d^2F}{dx^2} + \left(p_F^2 + \frac{n_y^2\epsilon^2}{x}\right)F\right\} = 0 \tag{53}$$

which, taking into account the conditions at infinity, is equivalent to the Whittaker equation for F

$$\frac{d^2F}{dx^2} + \left(p_F^2 - \frac{\epsilon^2 q_F^2}{x + \epsilon^2}\right)F \tag{54}$$

As anticipated, the singularity at $x = -\epsilon^2$ replaces the confluence with the Bernstein branch. Note also the cut–off at $x = \epsilon^2 n_y^2$, which exists also in the 4th order equation.

The general solution of (52)–(54) can be written

$$E_+ = \left(\frac{d}{dx} + n_y\right) Y_{\pm i\kappa, m}\left(\pm 2ip_F(x + \epsilon^2)\right) \tag{80}$$

where Y is any solution of Whittaker's equation with

$$\kappa = \frac{\eta}{\pi} \qquad m = \frac{1}{2} \tag{55}$$

(the signs in the argument and before κ must correspond). To obtain the connection formulas for the order–reduced problem we can now use the well–known asymptotic properties of Whittaker functions, taking into account that to satisfy causality the singularity at $x = -\epsilon^2$ must be bypassed from above.

A) Incidence from the low field side. In this case the solution on the high field side must be of the form:

$$E_+ = A\left(\frac{d}{dx} + n_y\right) W_{-i(\eta/\pi),m}\left(-2ip_F(x+\epsilon^2)\right) \tag{56}$$

with $\arg(-ip_F x) = \pi/2$ when $x < 0$, so that asymptotically

$$E_+ \sim A\left(-ip_F + n_y\right)\left\{e^{+\frac{\eta}{2}}\, e^{-i\left\{p_F(x+\epsilon^2) - \frac{\eta}{\pi}\ln\left(2p_F|x+\epsilon^2|\right)\right\}}\right\} \tag{57}$$

for large negative x: this is the transmitted FW. On the positive x–axis we will have $\arg(-ip_F x) = 3\pi/2$, which is outside the domain of validity of the usual asymptotic expansions. To overcome this difficulty we use a continuation formula for Wittaker functions, which we obtain starting from Eq. (13.1.10) of reference [12], and then eliminating $M_{i\kappa,1/2}$ using Eq. (1.9.9) of reference [13]:

$$\begin{aligned} W_{-i\kappa,\frac{1}{2}}\left(2p_F|x+\epsilon^2|\, e^{i\frac{3\pi}{2}}\right) =& e^{2\eta}\Big\{W_{-i\kappa,\frac{1}{2}}\left(-2ip_F(x+\epsilon^2)\right) \\ &+ \frac{\Gamma(1-i\kappa)}{\Gamma(1+i\kappa)}\, W_{+i\kappa,\frac{1}{2}}\left(+2ip_F(x+\epsilon^2)\right)\Big\} \end{aligned} \tag{58}$$

where now on the r.h. side $i = e^{\pm i(\pi/2)}$. Thus for large positive x we get

$$\begin{aligned} E_+ \sim A(-ip_F)\Big\{\zeta_- e^{+\frac{3\eta}{2}}\Big[&\epsilon^{-i\left\{p_F(x+\epsilon^2) - \frac{\eta}{\pi}\ln\left(2p_F(x+\epsilon^2)\right)\right\}} \\ &- \zeta_+ \frac{\Gamma(1-i\kappa)}{\Gamma(1+i\kappa)}\left(1-e^{-2\eta}\right)\epsilon^{+i\left\{p_F(x+\epsilon^2) - \frac{\eta}{\pi}\ln\left(2p_F(x+\epsilon^2)\right)\right\}}\Big]\Big\} \end{aligned} \tag{59}$$

From (58) and (59) we read the coefficients of reflection, transmission and absorption:

$$\begin{aligned} \mathcal{R} &= (1-e^{-2\eta})^2 \\ \mathcal{T} &= e^{-2\eta} \\ \mathcal{A} &= 1 - \mathcal{R} - \mathcal{T} = (1-e^{-2\eta})e^{-2\eta} \end{aligned} \tag{60}$$

Except for the interpretation of the "absorption coefficient" $\mathcal{A}$, they are identic with the results of the full FLR treatment.

B) Incidence from the high field side. In this case

$$E_+ = B\left(\frac{d}{dx} + n_y\right) W_{+i(\eta/\pi),m}\left(+2ip_F(x+\epsilon^2)\right) \tag{61}$$

Here $\arg(ip_F x) = \pi/2$ when $x > 0$, so that

$$E_+ \sim B\left(\frac{d}{dx} + n_y\right)\left\{e^{-\frac{\eta}{2}}\, e^{+i\left\{p_F(x+\epsilon^2) - \frac{\eta}{\pi}\ln\left(2p_F|x+\epsilon^2|\right)\right\}}\right\} \tag{62}$$

Here $\arg(ip_F x) = \pi/2$ when $x > 0$, so that

$$E_+ \sim B\left(\frac{d}{dx} + n_y\right)\left\{e^{-\frac{\eta}{2}}\, e^{+i\left\{p_F(x+\epsilon^2) - \frac{\eta}{\pi}\ln(2p_F|x+\epsilon^2|)\right\}}\right\} \tag{62}$$

for large positive x. For large negative x we will have $\arg(ip_F x) = -\pi/2$, so that we can still obtain the asymptotic expansion directly:

$$E_+ \sim B\left(\frac{d}{dx} + n_y\right)\left\{e^{+\frac{\eta}{2}}\, e^{+i\left\{p_F(x+\epsilon^2) - \frac{\eta}{\pi}\ln(2p_F|x+\epsilon^2|)\right\}}\right\} \tag{62}$$

for large negative x. Hence we find

$$\begin{aligned} \mathcal{R} &= 0 \\ \mathcal{T} &= e^{-2\eta} \\ \mathcal{A} &= 1 - \mathcal{R} - \mathcal{T} = 1 - e^{-2\eta} \end{aligned} \tag{63}$$

again in agreement with the FLR results.

The normalized causal solutions representing a fast wave incident from the low field (right) and high field (left) sides are shown in fig. 9 a) and b), respectively. From the relative amplitude and phase of the real and imaginary parts of E_+ one can qualitatively verify the validity of Eqs. (62) and (63): for example, it is clear that no reflection occurs for high field side incidence. The singularity at $x = -\epsilon^2$ is also clearly visible. This resonance has been introduced to replace mode conversion as a power sink, and is not by itself physically meaningful. We recall [8] that the wave equation describing cold ion–ion resonances can also be put in the form of a confluent hypergeometric equation. In that case, however, the wave electric field remains finite at the resonance, and only its derivative (i.e. the wave magnetic field) has a logarithmic singularity. Here, by contrast, the singularity affects already the electric field. As a consequence, the reduced equation cannot provide a good approximation to the solutions obtained in the previous section in the immediate vicinity of the spurious resonance. Nevertheless, the discrepancy is restricted to a narrow layer around the singularity, whose width can be estimated from the series expansion of Whittaker functions at the origin as half the distance between the singularity and the cyclotron harmonic:

$$|x + \epsilon^2| \lesssim \kappa = \frac{\epsilon^2}{2} \tag{64}$$

Apart for the omission of the BWs, therefore, the order reduction algorithm reproduces well the FW field pattern almost everywhere, and not only in the asymptotic region.

5 – First harmonic cyclotron absorption.

Direct cyclotron damping at the first harmonic can be easily estimated in the two limits of weak and strong damping; an interpolation formula between the two cases is then suggested by the considerations of section (2.2) about the transition between the mode conversion and the cyclotron damping regimes.

A) Weak damping limit. For nearly perpendicular propagation we can estimate FH cyclotron damping per transit perturbatively, starting from

$$\Delta P_x = -\int_{-\infty}^{+\infty} \mathrm{Im}\,(\lambda_2) \left| \left(\frac{d}{dx} - n_y \right) E_+ \right|^2 dx \tag{65}$$

To evaluate the field, we assume that the order reduction approximation gives a good estimate also near the cyclotron harmonic resonance, as suggested by Eq. (64). Using (52)–(54) we have

$$\left| \left(\frac{d}{dx} - n_y \right) E_+ \right|^2 = \left| \left(\frac{d^2}{dx^2} - n_y^2 \right) F \right|^2 = \left(\frac{q_F^2\, x}{x + \epsilon^2} \right)^2 |F|^2 \tag{66}$$

To avoid interference with the spurious resonance at $x = -\epsilon^2$ we must impose $\Delta\, x_{cycl} \ll \epsilon^2$, or

$$|n_\parallel| \frac{v_{thi}}{c} \ll \frac{\beta_i}{4} \tag{67}$$

This is the condition discussed in section 2.2, which characterizes the mode conversion regime. When it is satisfied, using the appropriate normalizations we finally get:

$$\frac{\Delta P_x}{P_x} \simeq \frac{\pi}{4} \beta_i \left(-\frac{\nu_R^2}{\nu_S^2} \right)^2 (k_o q_F R_o) \left(\frac{n_\parallel \frac{v_{thi}}{c}}{\frac{1}{4}\beta_i \left(-\frac{\nu_R^2}{\nu_S^2} \right)^2} \right)^2 |F_o(\eta)|^2 \tag{68}$$

where

$$|F_o(\eta)|^2 = \begin{cases} e^{\eta} \left| W_{-i\frac{\eta}{\pi},\frac{1}{2}}(-4i\eta) + \frac{\Gamma(1-i(\eta/\pi))}{\Gamma(1+i(\eta/\pi))} W_{+i\frac{\eta}{\pi},\frac{1}{2}}(+4i\eta) \right|^2 & \text{lfs incidence} \\ e^{-\eta} \left| W_{+i\frac{\eta}{\pi},\frac{1}{2}}(+4i\eta) \right|^2 & \text{hfs incidence} \end{cases} \tag{69}$$

The factors $|F_o(\eta)|^2$ are shown in fig. 10. Since η is practically always much smaller than unity, however, the approximations $|F_o|^2 = 4$ for low field side incidence, and $|F_o|^2 = 1$ for high field side incidence, are usually sufficient. Note that in spite of the apparently anomalous behaviour of (68) for $\beta_i \to 0$ there is no singularity, since the this limit is incompatible with the mode–conversion regime: the fraction in parenthesis is bound to be small by condition (67).

B) ICR absorption in the limit of strong damping. In the opposite limit,

$$n_\parallel \frac{v_{thi}}{c} \gg \frac{\beta_i}{4} \tag{70}$$

Doppler broadening of the cyclotron resonance washes out the Bernstein wave confluence, and the WKB solution can be used to estimate damping through the cyclotron layer:

$$\Delta P_x \simeq -q_F^2 |E_+|^2 \int_{-\infty}^{+\infty} \mathrm{Im}\,(\lambda_2)\, dx = \frac{\pi}{2} \beta_i (k_o R_o)\, q_F^2 |E_+|^2 \tag{71}$$

or, using Eqs. (25),

$$\frac{\Delta P_x}{P_x} \simeq \alpha_{fh} = \frac{\pi}{4} \beta_i \left(-\frac{\nu_R^2}{\nu_S^2} \right)^2 (k_o q_F R_o) \tag{72}$$

C) Interpolation formula. We cover both regimes by using an effective value for α_{hf} given by

$$\alpha_{eff} = \alpha_{fh} \cdot \frac{\delta_{fh}^2}{1 + \delta_{fh}^2} \tag{73}$$

where α_{fh} is the first harmonic IC absorption at large $n_\parallel$, and the parameter

$$\delta_{fh}^2 = \frac{2 n_\parallel^2 \frac{v_{thi}^2}{c^2}}{\left[\beta_i \left(-\frac{\nu_R^2}{\nu_S^2} \right)^2 \right]^2} \tag{74}$$

characterizes the transition from the mode conversion regime ($\delta_{fh}^2 \ll 1$) to the cyclotron damping regime ($\delta_{fh}^2 \gg 1$).

For simplicity, we have ealuated α_{fh} assuming $|E_+|$ to be roughly constant throughout the absorption region. When IC damping is strong, however, this parameter can become comparable or even larger than unity. A better approximation, which avoids this inconsistency, is to write

$$\frac{\Delta P_x}{P_x} \simeq 1 - \exp\left(-\alpha_{eff}\right) \tag{75}$$

D) Suppression of mode conversion by IC damping. With increasing $n_\parallel$, as cyclotron damping increases, mode conversion decreases with respect to its value at perpendicular propagation, and is completely suppressed when condition (69) is satisfied. We can describe this transition by writing

$$A(n_\parallel) \simeq A(0)\, e^{-\delta_{fh}^2} \tag{76}$$

For waves incident from the low field side and $\delta_{fh} \ll 1$ this expression can be easily justified by assuming that cyclotron damping simply depletes the power which can reach the mode conversion layer. The generalization to larger values of δ_{fh} is made by analogy to the one leading to Eq. (74).

6 – Examples.

We summarize here the parameters of ASDEX Upgrade and ITER which were used in the examples:

TABLE 1

	ASDEX U.	ITER (T)	(D)
Toroidal radius	1.65 m	7.75 m	
Plasma radius	0.5 m	2.25 m	
Magnetic field on axis	2 T	6 T	
Central density	$5\ 10^{19}$ m^{-3}	$1.4\ 10^{20}$ m^{-3}	
Central temperature	2 to 8 keV	5 to 20 keV	
Frequency	60 Mhz	60.1 Mhz	(91 Mhz)

In fig. 11 the fractional power absorbed at the FH IC resonance according to Eq. (75) is plotted versus n_ϕ for the low density, low temperature ASDEX Upgrade plasma. Also shown are results obtained numerically with the finite–element code FELICE [19], which solves the complete FLR wave equations in slab geometry. To simulate the idealized analytic situation with FELICE, the density and temperature were assumed radially constant, and only the horizontal variation of the magnetic field was retained; the electron temperature was reduced to 0.1 keV to eliminate damping on the electrons, and collisional damping as well as stochastic ion damping of the Bernstein waves were switched off. The waves are launched from the low field side, and outward radiation conditions (equivalent to matching to the outgoing WKB solutions) are then imposed 25 cm to the inside of the cyclotron resonance (this procedure was stopped at $n_\phi \simeq 40$ ($n_\parallel \simeq 20$), because the fast wave approaches the $n_\parallel^2 = R$ cutoff at the plasma density of the example). The code then provides the fractions of power absorbed in the IC resonance layer, and radiated in the fast and Bernstein waves; the latter is identified with the mode conversion efficiency. The agreement between analytic and numerical results is excellent. It should however be realized that the two approaches are not completely equivalent, as will be discussed below.

At first sight, the decrease of α_{eff} at large $n_\parallel$ might appear surprising: since the integral of $\mathrm{Im}\lambda_2$ across the resonance layer is independent from $n_\parallel$, one would rather expect α_{eff} to reach a constant value in the cyclotron damping regime. The decrease however is due to the factor q_F in α_{hf}, which is a decreasing function of $n_\parallel$, and approaches zero as the R–cutoff is approached. The fact that this prediction of the analytic theory is confirmed by the numerical results gives confidence in the estimates

of IC absorption made in this section. The same good agreement is found in a scan over temperature at constant n_ϕ, fig. 12.

In fig. 13 the fractional absorption by FH IC damping predicted by Eq. (75) is plotted for ASDEX Upgrade, and in figs. 14 for Tritium heating in ITER, at different temperatures. It is interesting to note that the heating efficiency in the ASDEX Upgrade example is larger than that of the ITER/Tritium cases: the latter might be marginal below 5 keV (first harmonic heating of deuterium would be much more favorable). The rapid increase of damping with temperature is evident in both cases. It should also be kept in mind that, once heating has begun, the production of a population of fast ions will further boost the absorption efficiency. The investigation of this quasilinear effects, however, requires information from the solutions of the Fokker–Planck equation, and is postponed to a future report.

The comparison of the analytic and numeric mode conversion efficiency appears at first less satisfactory, as shown in fig. 15 for the low density ASDEX Upgrade case at 2 keV. The width of the mode conversion regime, as determined by the exponential factor in δ_{hf}^2 added in Eq. (76), is very well reproduced. The numerically evaluated mode conversion efficiency at perpendicular propagation, however, exceeds the theoretical one by a factor of 2. In the example the optical thickness η is close to the value $\eta_{opt} = \log 2$ for which $\mathcal{A} = 0.25$ takes its maximum possible value for low field side incidence. To explain how the numerically evaluated efficiency can exceed this theoretical maximum we must exhamine more in details the difference between the numeric and the analytic approach.

In FELICE a few small FLR terms which were neglected in Eq. (1) are retained. Moreover, even if density and temperature gradients are made to vanish, gradients in Ω_i are retained in all coefficients, rather than in the resonant term λ_2 only, as in the analytic approximation. None of these differences, however, is likely to be important. The discrepancy must be attributed to the boundary conditions imposed on the incidence side. In FELICE, which is a code written for the investigation of IC antennas, a metallic wall is assumed at some distance from the the plasma edge. As a consequence, the solution chosen by FELICE is not the same as the one used to derive Eq. (76). Eigenmodes with large standing wave ratio can be excited between the cutoff associated to the mode conversion layer and the wall. The value of $|E_+|^2$ in the numerical solutions therefore depends sensitively on how close the parameters of a given run match those of an eigenmode. The interpretation in terms of eigenmodes is clearly confirmed by fig. 16, which shows a temperature scan of the mode conversion efficiency for low magnetic field side perpendicular incidence in ASDEX Upgrade.

We could easily modify Eq. (76) to take into account metallic boundary conditions at an appropriate distance from the mode conversion layer. It should be realized, however, that the importance of eigenmodes is much exaggerated by the slab geometry assumed.

A better procedure to improve agreement between the analytic and numerical results consists in summing the geometric series for the wave reflected back and forth between wall and cutoff; this amounts to substitute $\mathcal{A}$ with

$$\mathcal{A}' = \frac{\mathcal{A}}{1-\mathcal{R}} \tag{77}$$

This of course does not take into account the phase relations which periodically enhance or reduce $|E_+|^2$ at the cyclotron resonance. Nevertheless, as shown by curve b) in fig. 15, $\mathcal{A}'$ gives a fair average over the peaks and valleys of the numerical results. In particular, $\mathcal{A}'$ reproduces correctly the fact that the numerical mode conversion does not decrease to zero at large temperatures: this is because the decrease of $\mathcal{A}$ is compensated by $\mathcal{R}$ approaching unity. In tokamak geometry a similar averaging will be automatically performed, since for a given n_ϕ many poloidal modes m_ϑ with different relations to eigenmodes are simultaneously excited [5]. Thus Eq. (77) is likely to be a better approximation than the numerical integration of the wave equations in slab geometry. A procedure equivalent to the one leading to Eq. (77) has been used in ICEVAL [20], a routine which allows a very fast yet accurate analysis of IC heating scenarios in tokamaks.

The reason of the good agreement between the analytic and numerical results for cyclotron damping is also clear: $\mathcal{R}$ is nearly zero in the cyclotron damping regime. Eigenmodes of the kind just described can be excited only for low $n_\parallel$, satisfying condition (66).

Figs. 17 and 18 show $\mathcal{A}$ versus n_ϕ for low field incidence at various temperatures for ASDEX Upgrade and ITER. In Asdex, mode conversion efficiency is nearly maximum at 2 keV; hence, as T_i increases, $\mathcal{A}(n_\phi)$ broadens but decreases. In ITER, on the other hand, $\mathcal{A}$ reaches its maximum only at large temperature, $T_i \gtrsim 20$ keV. On the other hand, in terms of $n_\parallel$, the range in which mode conversion takes place is much narrower in ITER than in ASDEX Upgrade, in agreement with the results of figs. 5 and 6.

7 – Conclusions.

By solving the linear wave equations near the first harmonic of the ion cyclotron frequency, we have obtained simple analytic expressions for the fractional IC absorption and mode conversion in this heating scenario. The analytic results have been found to be in excellent agreement with numerical simulations. They can be conveniently used for a reliable first estimate of the heating efficiency of a given experimental setup, preliminarly to more sophisticated simulations.

We have identified to regimes, one dominated by mode conversion, the other by cyclotron damping, analogous to those which characterize IC minority heating. The cyclotron regime, which requires a sufficiently large $n_\parallel$, is more favorable for plasma

heating, since it corresponds to larger fractional absorbtion per transit, and avoids eigenmodes which can adversely affect the mode conversion regime. The critical value of $n_\parallel$ increases with temperature, but is always relatively small; antisymmetric antennas can easily be made to radiate mostly in the cyclotron damping regime. In addition to give quantitative information on well–known dependencies of the heating efficiency on the partial ion pressure, $n_\parallel$, the toroidal radius, and other plasma parameters, the analytic results also stress the importance of coefficients that depend on the plasma composition. Thus, in spite of the higher temperature and larger major radius, first harmonic heating of Tritium in ITER is found to be somewhat less easy that first harmonic heating of Hydrogen in ASDEX Upgrade. First harmonic heating of Deuterium in ITER would be much more favorable; unfortunately it has several disadvantages (interaction with α particles and with Hydrogen contamination, higher frequency).

The analysis performed here is obviously incomplete, since it is confined to the linear theory, and neglects the quasilinear modifications of the ion distribution function under the effect of heating. In turn, the production of a sufficient number of suprathermal ions will favorably influence absorption. A frame for the description of the effects of deviations from thermal equilibrium on wave propagation and absorption is being developed [21]–[22]. To use it within an analytic approach, however, one needs information about the solution of the Fokker–Planck equation; a separate investigation of the quasilinear effects is underway.

Aknowledgments. The content of section 3 is largely based on work made in collaboration with Dr. M. Ottaviani during the preparation of [8].

References.

[1] Bernstein I.B., Waves in a Plasma in a magnetic field. Phys. Rev. **109** (1958) 10.

[2] Weynants R.R., Ion Heating at twice the ion cyclotron frequency in reactor oriented machines. Phys. Rev. Lett. **33** (1974) 78.

[3] Ram A., Bers A., Electron Heating by mode-converted Ion Bernstein Waves in ICRF Heating of Tokamak plasmas, Proc. 7th Top. Conf. on Applications of RF Power to Plasmas, Kissimmee (Fl., USA) 1987, p. 378.

[4] Riyopoulos S., Nonlinear Landau damping of purely perpendicularly propagating Bernstein modes. J. Plasma Phys. **36** (1986) 111.

[5] Brambilla M., Krücken T., Numerical simulation of ion cyclotron heating of hot tokamak plasmas. Nucl. Fus. **28** (1988) 1813.

[6] Gambier D.J.D, Schmitt J.P.M., A solution to the linear wave conversion problem in weakly inhomogeneous plasmas. Phys. Fluids **26** (1983) 2200.

[7] Stix T.H., Swanson D.G., Propagation and mode conversion for waves in non-uniform plasmas. In: Handbook of Plasma Physics (A. Galeev, R.N. Sudan Ed.), North Holland 1985, Vol. 1, p.335, and references therein.

[8] Brambilla M., Ottaviani M., Mode Conversion near Ion-Ion Hybrid and IC Harmonic Resonances in Tokamaks.Plasma Phys. Contr. Fus. **27** (1985) 1.

[9] Chiu S.C., Analytic mode conversion calculations for the full wave equations at the ion second harmonics. Phys. Fluids **28** (1985) 2808.

[10] Budden K.G., Radio Waves in the Ionosphere, Cambridge Univ. Press (London) 1961.

[11] Lashmore-Davies C.N., Fuchs V., Francis G., Ram A.K., Bers A., Gauthier L., A theory of fast wave absorption, transmission and reflection in the ion cyclotron range of frequencies. Phys. Fluids **31** (1988) 1614, and references therein.

[12] Swanson D.G., Derivation of the mode conversion-tunneling equation from the Vlasov equation, Phys. Fluids **24** (1981) 2035.

[13] Colestock P.L., Kashuba R.J., The theory of mode conversion and wave damping near the ion cyclotron frequency, Nucl. Fus. **23** (1983) 763.

[14] Ottaviani M., Larmor radius expansion for the warm-plasma dielectric tensor, Lett. Nuovo Cimento **42** (1985) 385.

[15] Martin Th., Vaclavik J., Dielectric Tensor operator of a Nonuniformly magnetized Inhomogeneous Plasma., Helv. Phys. Acta **60** (1987) 471.

[16] Brambilla M., Finite Larmor radius wave equations in tokamak plasmas in the ion cyclotron frequency range, Plasma Phys. Contr. Fus. **31** (1989) 723.

[17] Abramowitz, M., Stegun I.A., Handbook of Mathematical Functions, Nat. Bureau of Standards (Washington, D.C.) 1964.

[18] Slater L.J., Confluent Hypergeometric Functions, Cambridge Univ. Press (England) 1960.

[19] Brambilla M., Theory of Bernstein Wave coupling with loop antennas, Nucl. Fus. **28** (1988) 549.

[20] Brambilla M., An improved routine for the fast estimate of ion cyclotron heating efficiency in Tokamak plasmas, Report IPP 5/44, February 1992.

[21] Van Eester D., The dielecric tensor for an arbitrary distribution function. Plasma Phys. Contr. Fus. **35** (1993) 441.

[22] Brambilla M., Hoffmann C., Self–consistent modeling of IC minority heating, 20th EPS Conf. on Controlled Fusion and Plasma Physics, Lissabon 1993, Vol. III, p. 957.

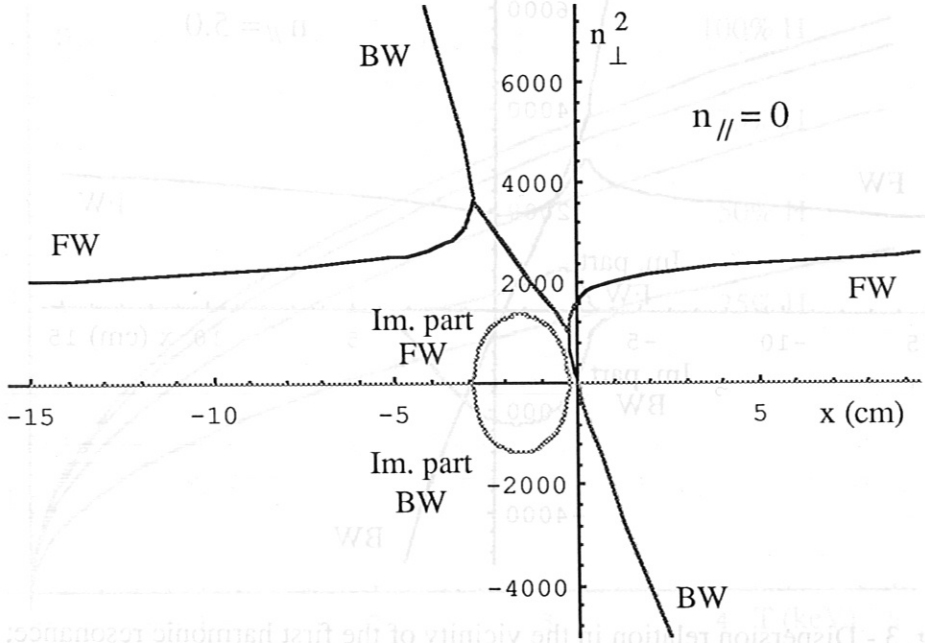

Fig. 1 - Dispersion relation in the vicinity of the first harmonic resonance; ASDEX Upgrade, $n_e = 5\ 10^{13}\ cm^{-3}$; B = 2 T; T = 2 keV; f = 60 Mhz (100% H), perpendicular propagation.

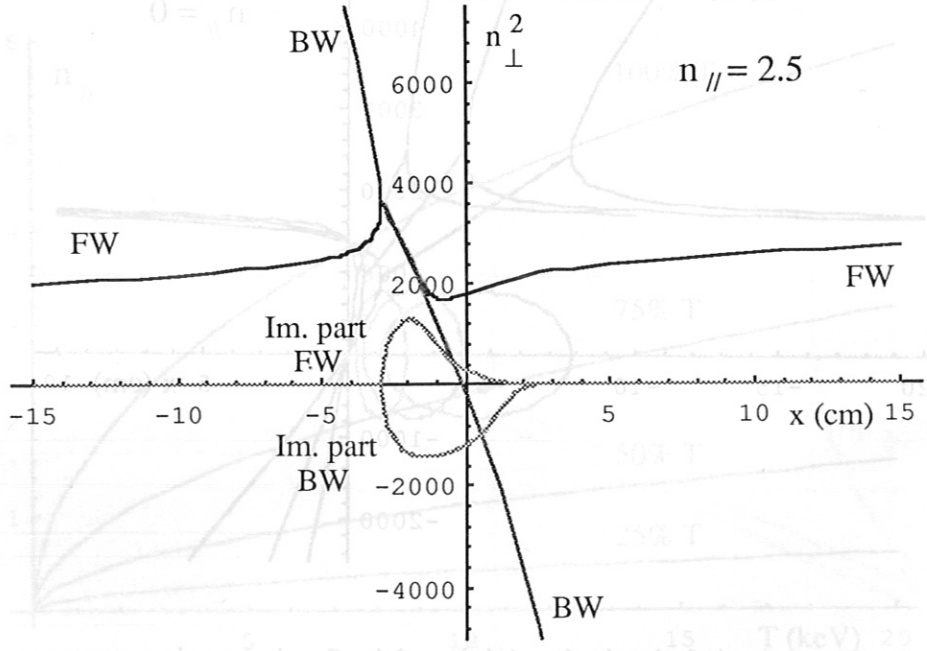

Fig. 2 - Dispersion relation in the vicinity of the first harmonic resonance; ASDEX Upgrade, $n_e = 5\ 10^{13}\ cm^{-3}$; B = 2 T; T = 2 keV; f = 60 Mhz (100% H), $n_{//} = 2.5$.

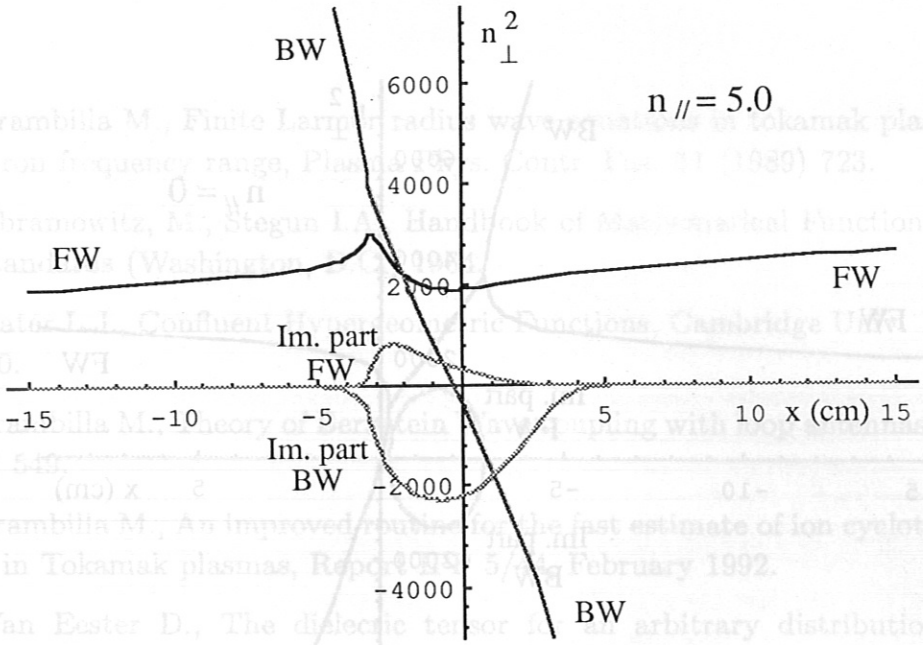

Fig. 3 - Dispersion relation in the vicinity of the first harmonic resonance; ASDEX Upgrade, $n_e = 5\ 10^{13}\ cm^{-3}$; B = 2 T; T = 2 keV; f = 60 Mhz (100% H), $n_{//} = 5.0$.

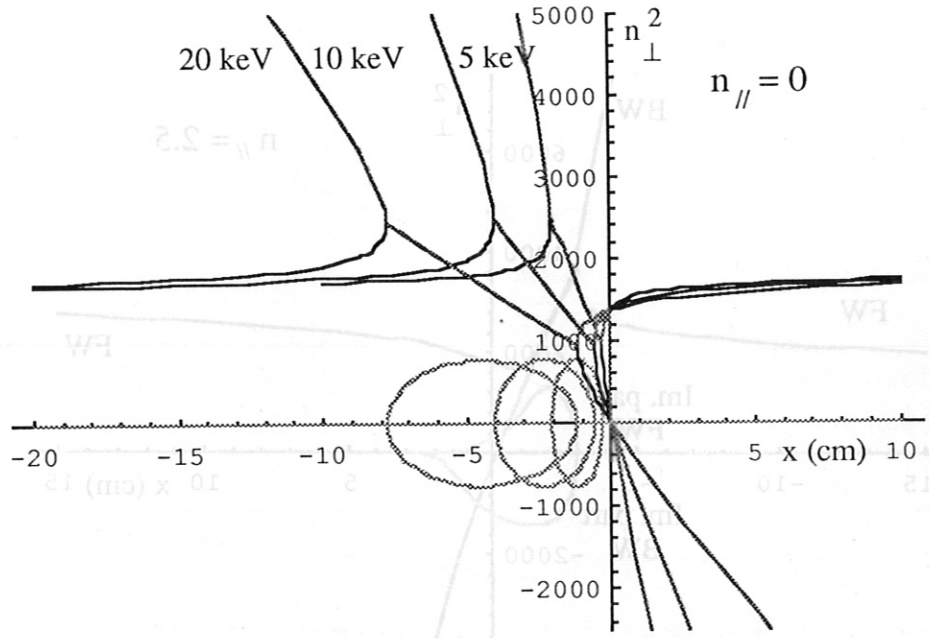

Fig. 4 - Dispersion relation in the vicinity of the first harmonic resonance; ITER, $n_e = 1.4\ 10^{14}\ cm^{-3}$; B = 6 T; 50% D, 50% T, f = 60.1Mhz (first harmonic of Tritium), perpendicular propagation.

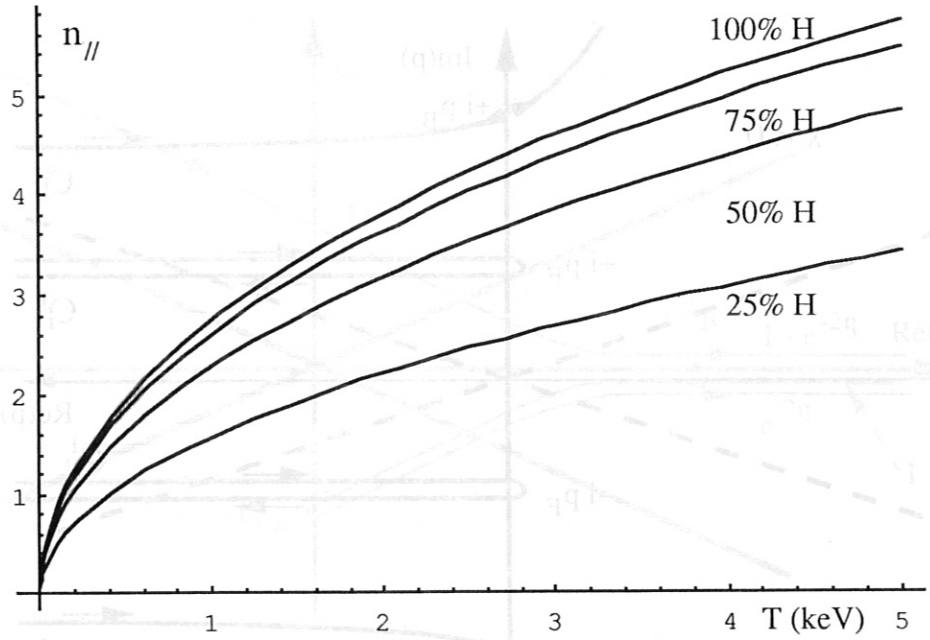

Fig. 5 - Critical $n_{//}$ vs temperature, ASDEX Upgrade, $n_e = 5\ 10^{13}\ cm^{-3}$; B = 2 T; H-D plasma; f = 60 Mhz.

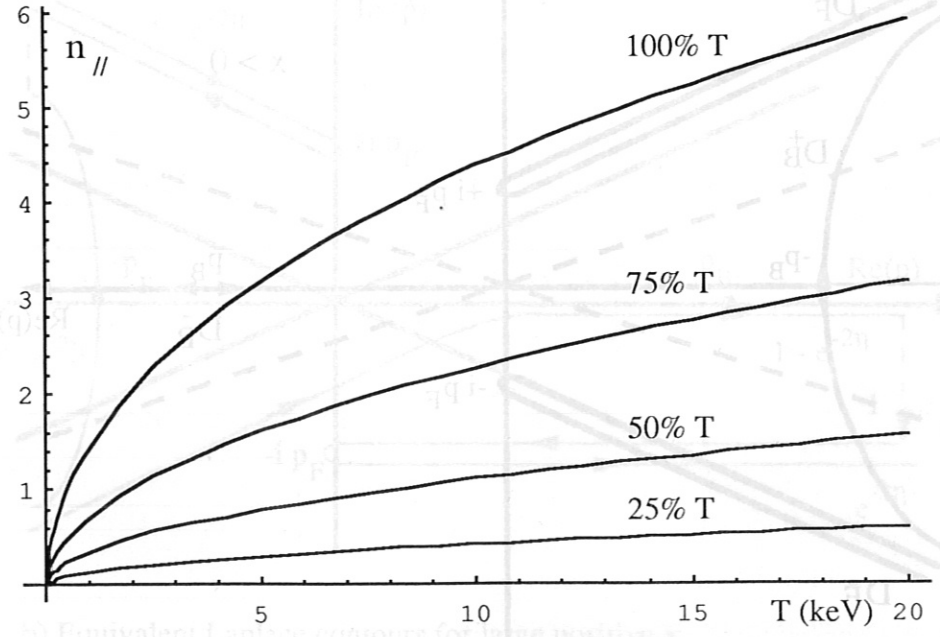

Fig. 6 - Critical $n_{//}$ vs temperature, ITER, $n_e = 1.4\ 10^{14}\ cm^{-3}$; B = 6 T; f = 60.1 Mhz (first harmonic of Tritium).

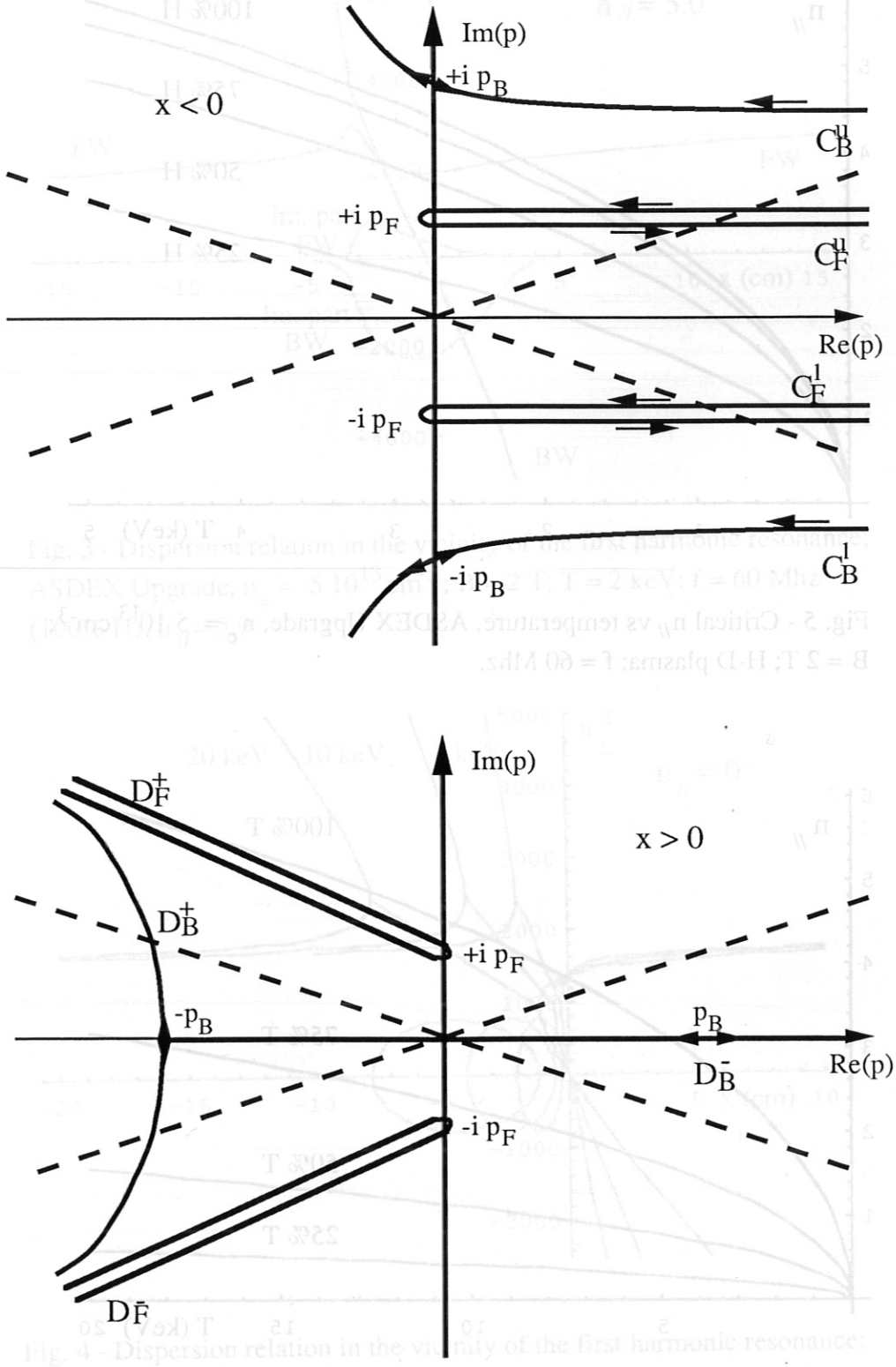

Fig. 7 - Laplace contours in the p-plane for the solution of the wave equations near the first cyclotron harmonic resonance.

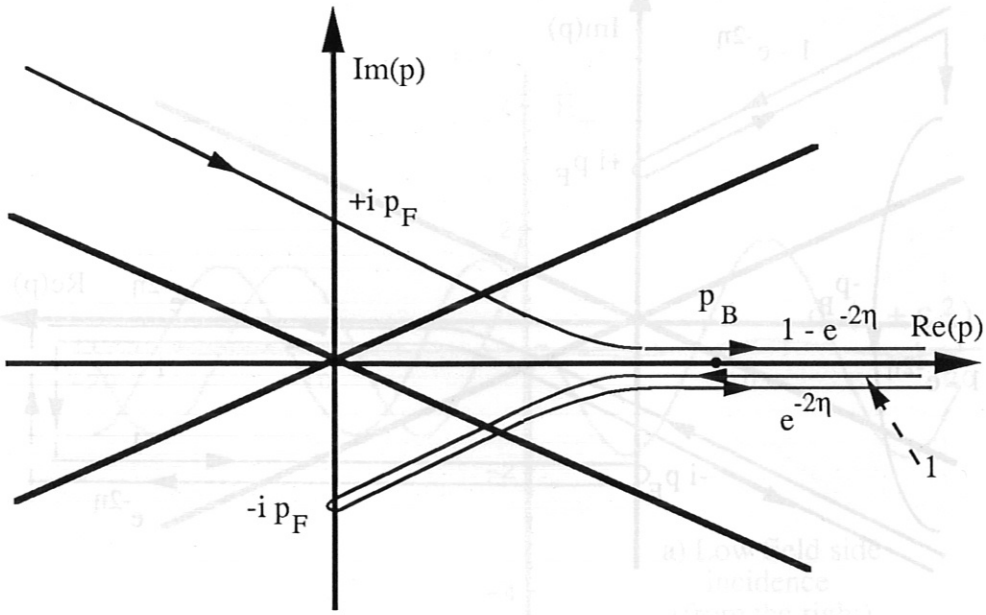

a) Weighted Laplace contours for large positive x to eliminate the growing Bernstein wave solution.

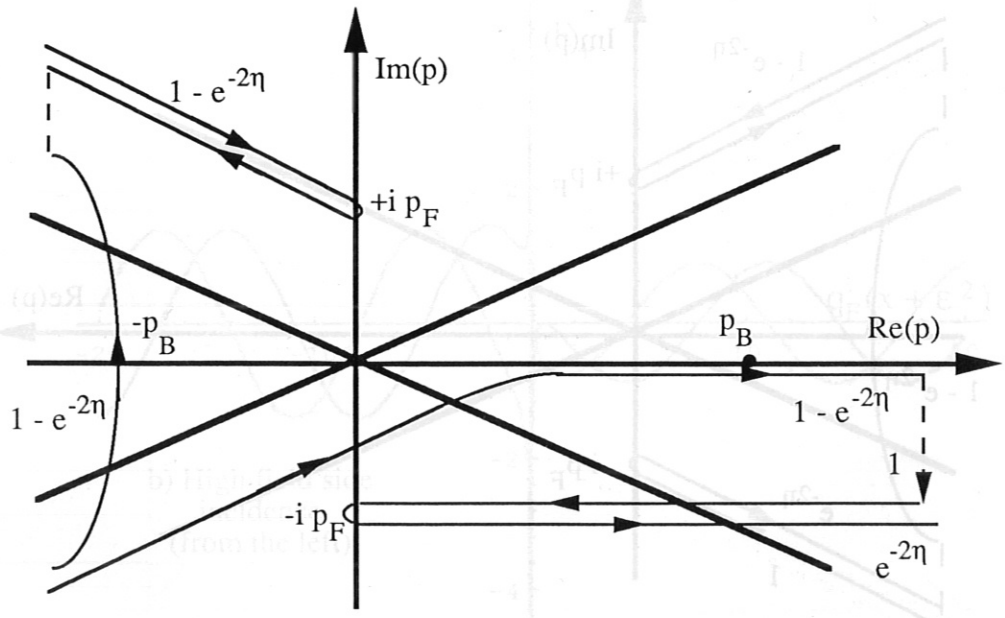

b) Equivalent Laplace contours for large positive x.

Fig. 8 - Laplace contours to obtain the connection formulas for low field side incidence.

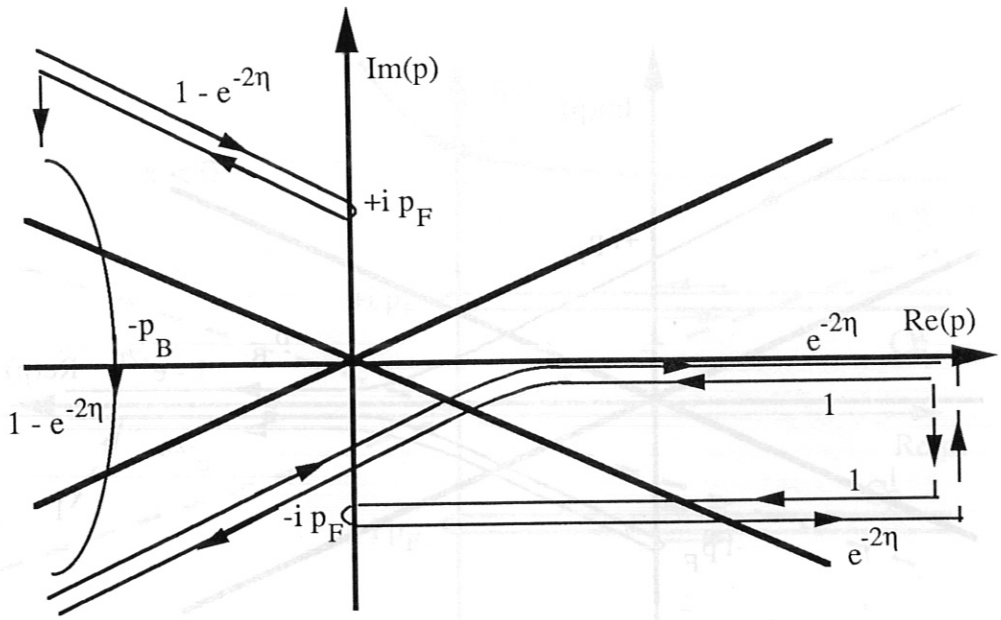

c) An equivalent representation of the contours. Draw the contours in the lower half-plane towards the left to get the next diagram.

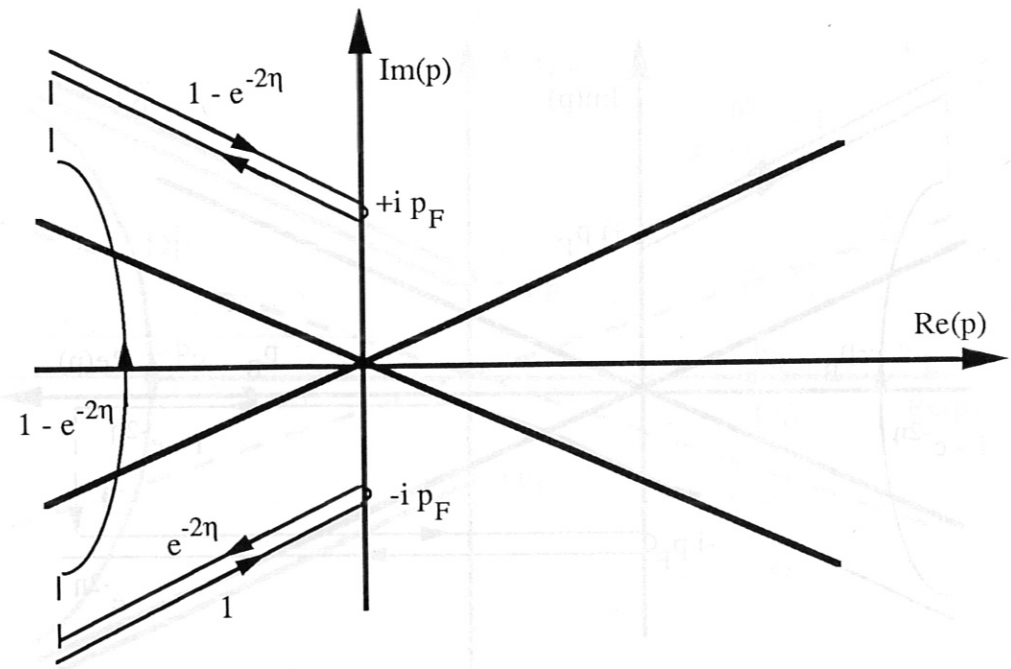

d) Final deformation of the Laplace contours, which gives the weighted solutions for large negative x.

Fig. 8 - Laplace contours to obtain the connection formulas for low field side incidence.

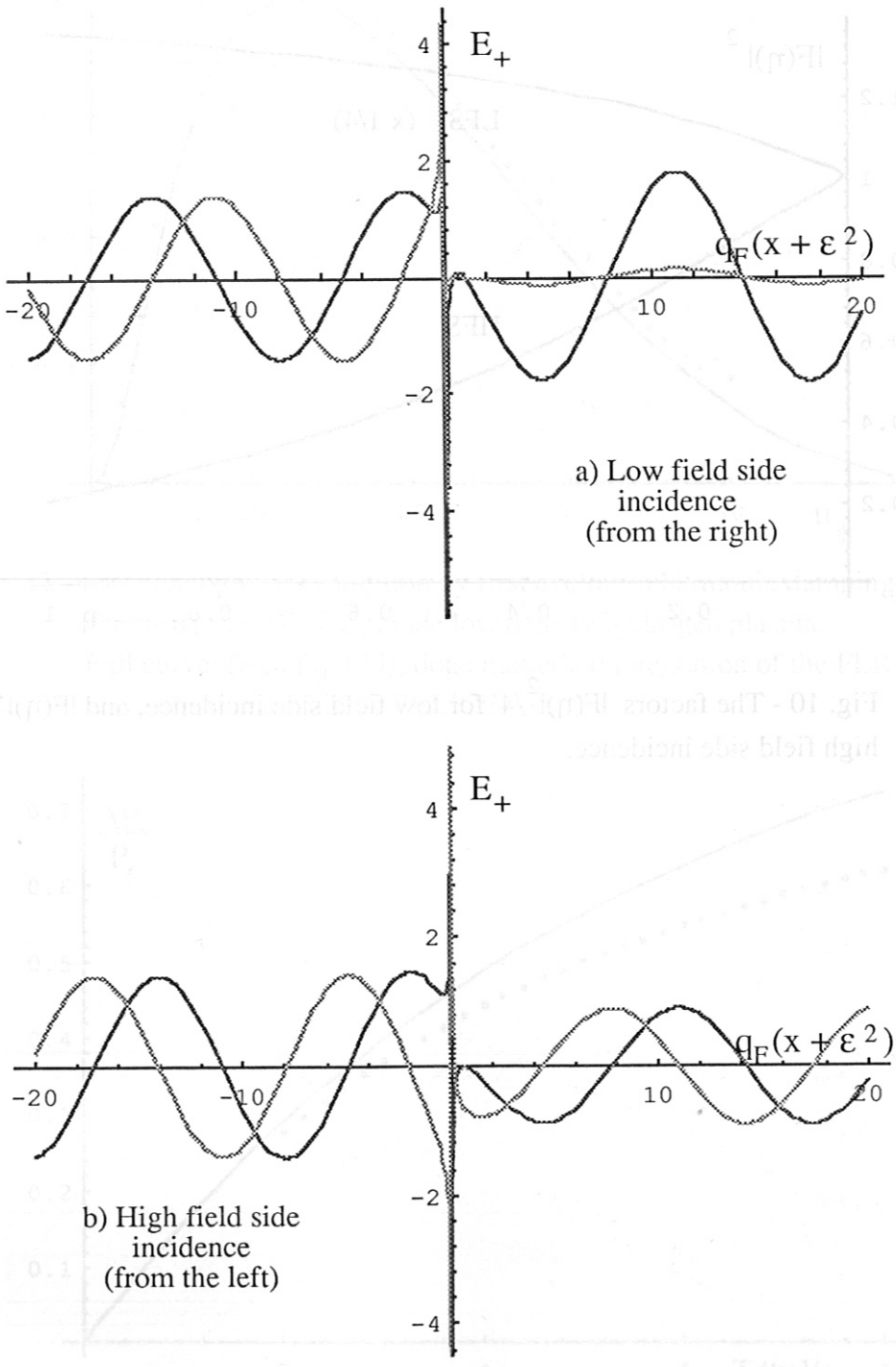

Fig. 9 - Causal solutions of the reduced wave equations. ASDEX Upgrade low density plasma, $\eta = 0.418$.

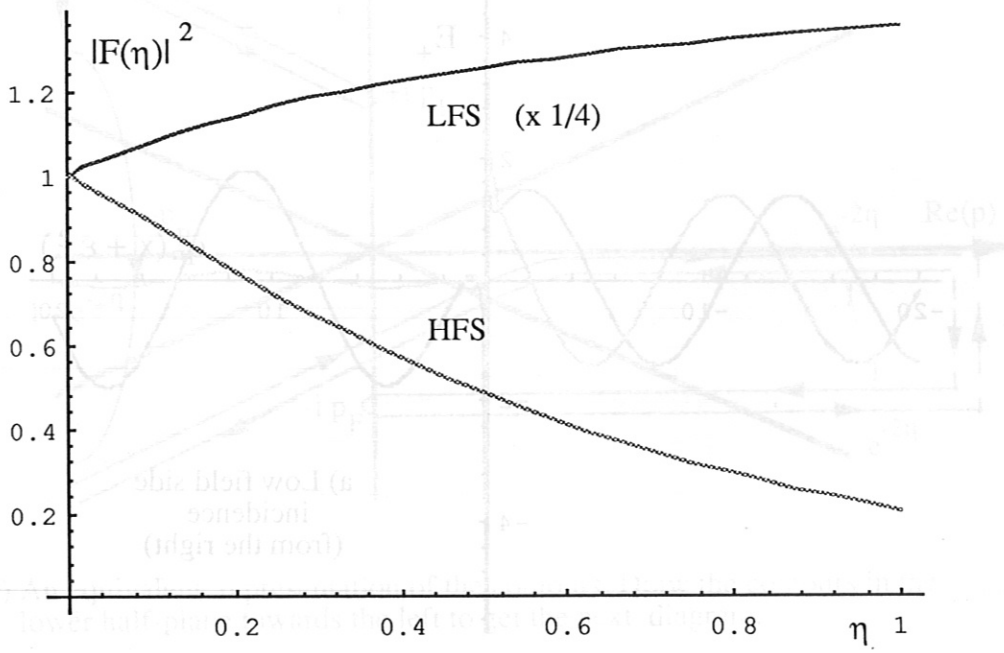

Fig. 10 - The factors $|F(\eta)|^2/4$ for low field side incidence, and $|F(\eta)|^2$ for high field side incidence.

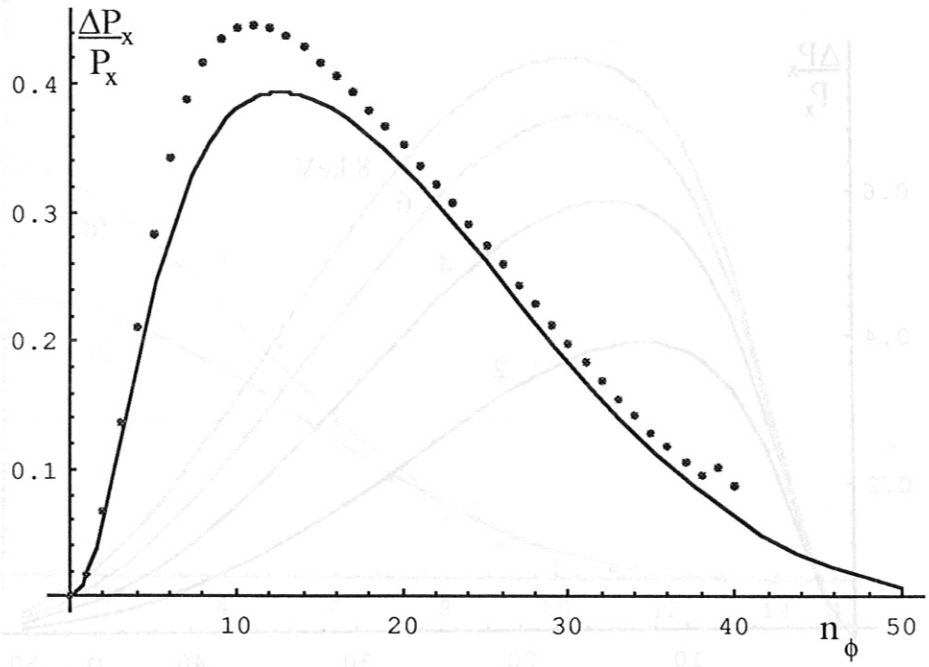

Fig. 11 - Fractional power absorption by first cyclotron harmonic damping versus n_ϕ; ASDEX Upgrade low density hydrogen plasma. Full curve: from Eq. (75); dots: numerical integration of the FLR wave equations with the FELICE code.

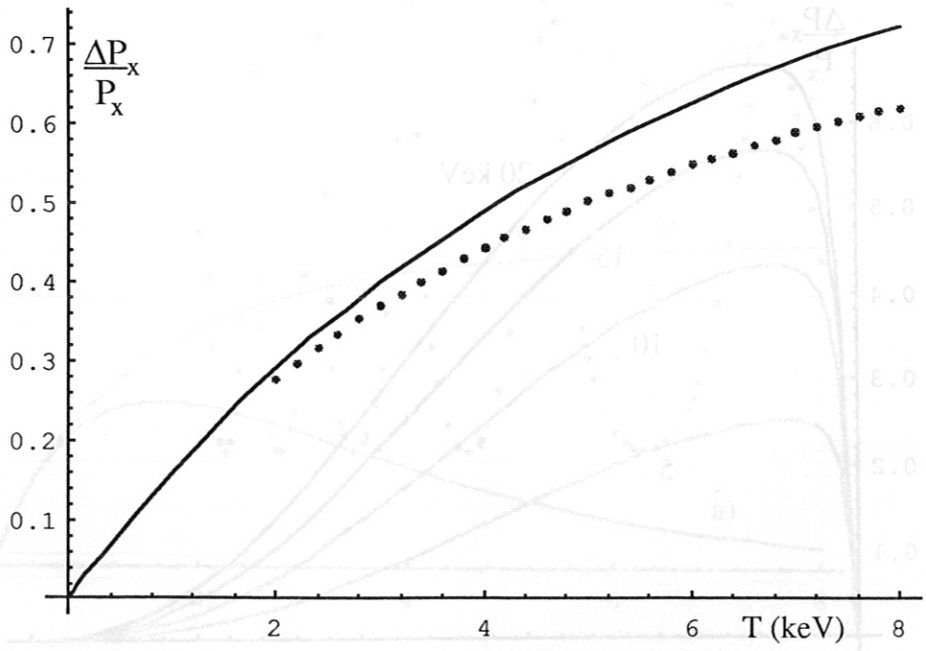

Fig. 12 - Fractional power absorption by first cyclotron harmonic damping versus temperature, $n_\phi = 25$; ASDEX Upgrade hydrogen plasma. Full curve: from Eq. (75); dots: numerical integration of the FLR wave equations with the FELICE code.

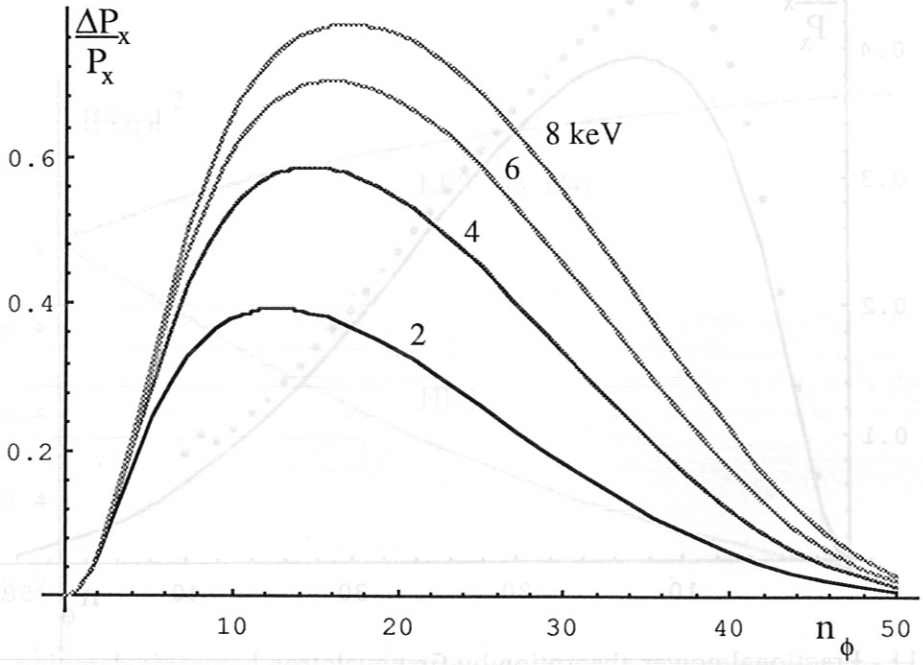

Fig. 13 - Fractional IC absorption at the first harmonic versus n_ϕ for the ASDEX Upgrade low density plasma at different temperatures.

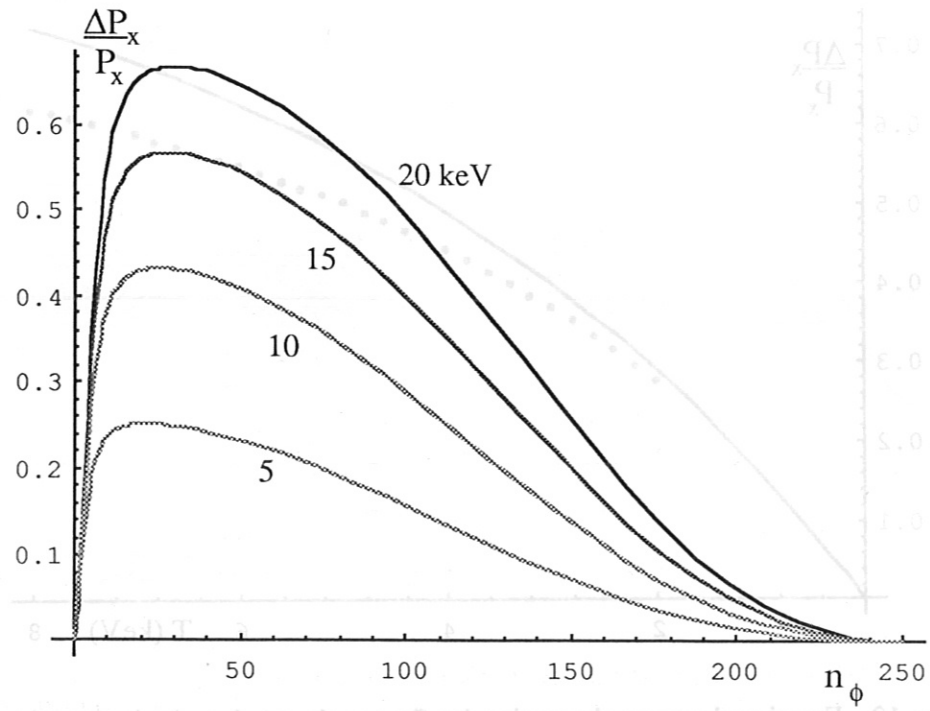

Fig. 14 - Fractional IC absorption at the first harmonic of Tritium versus n_ϕ for ITER at different temperatures

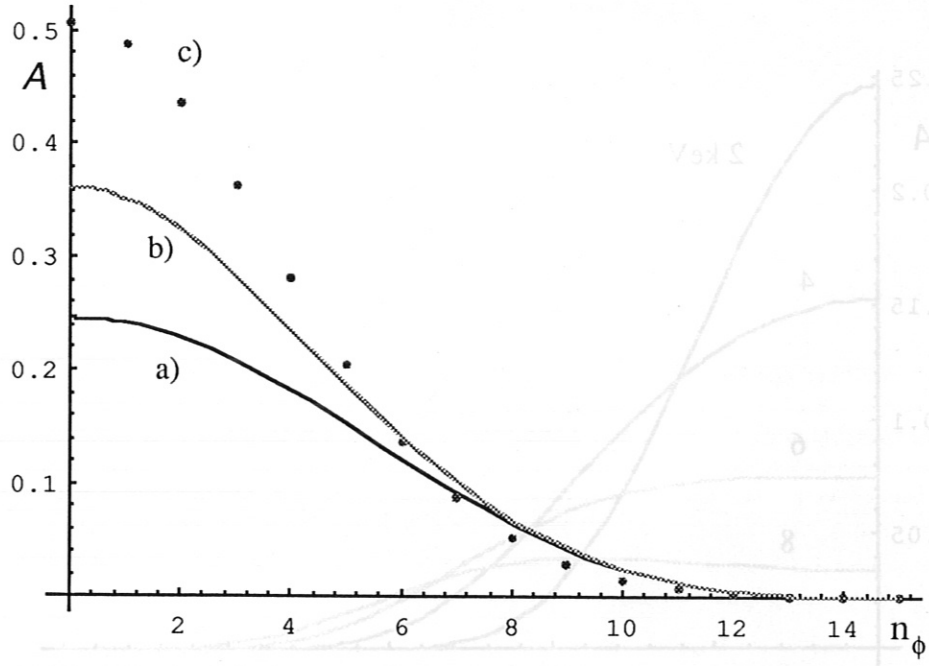

Fig. 15 - Mode conversion efficiency for low field side incidence, versus n_ϕ ; low density ASDEX Upgrade plasma, T_i = 2 keV, a) from Eq. (76); b) taking reflection into account, Eq. (77); c) the dots are numerical results from the FELICE code.

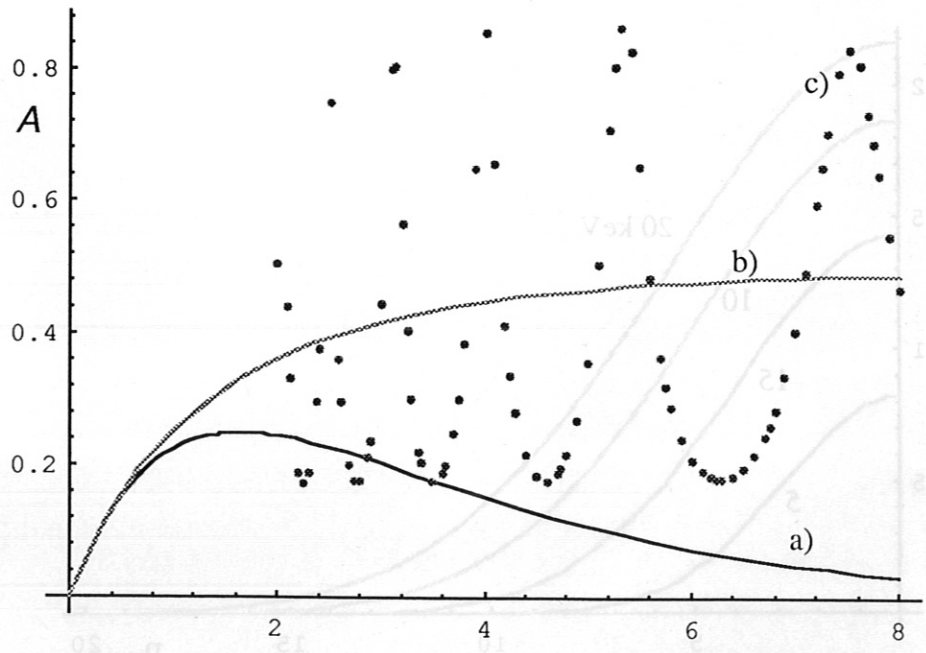

Fig. 16 - Mode conversion efficiency for low field side incidence, perpendicular propagation, versus temperature. Low density plasma, ASDEX Upgrade. a) from Eq. (76); b) taking reflection into account, Eq. (77); c) the dots are numerical results from the FELICE code.

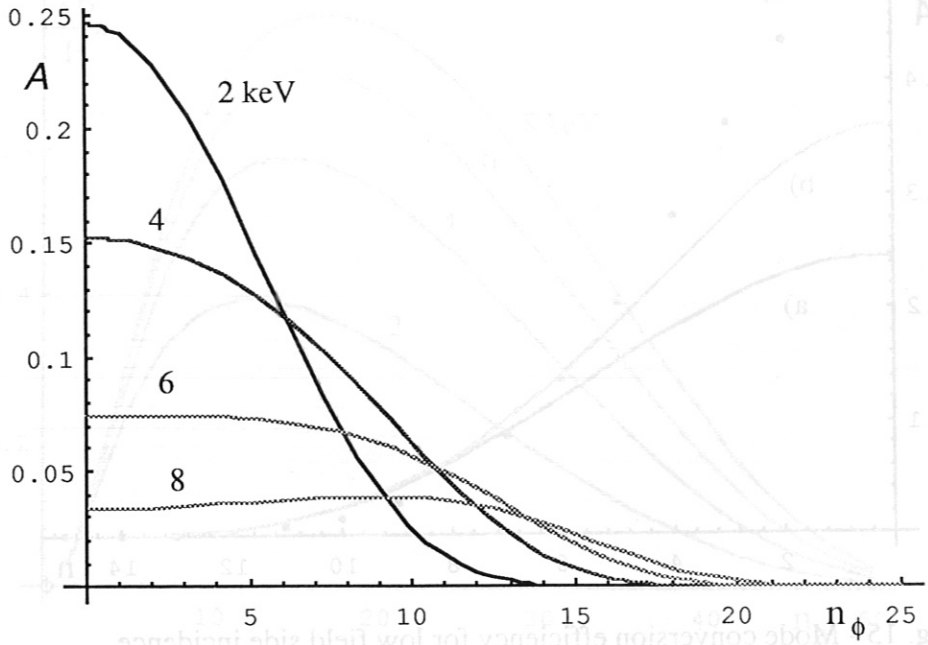

Fig. 17 - Analytic mode conversion efficiency versus n_ϕ for low field incidence; low density ASDEX Upgrade plasma at different temperatures.

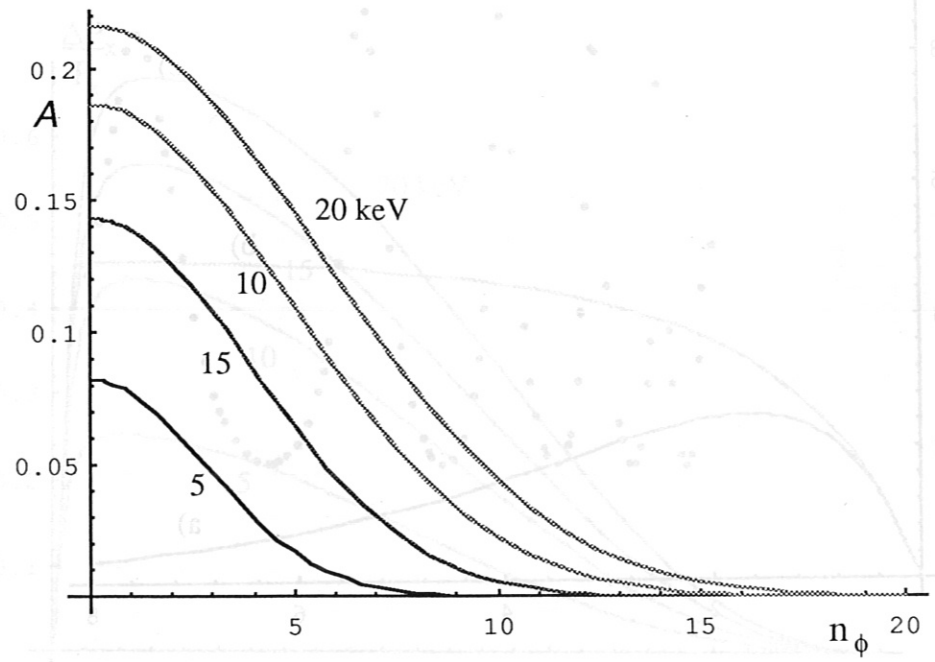

Fig. 18 - Analytic mode conversion efficiency versus n_ϕ for low field incidence; ITER first harmonic heating of Tritium, at different temperatures.